Nucleolar localization of the yeast RNA exosome subunit Rrp44 hints at early pre-rRNA processing as its main function

Received for publication, March 24, 2020, and in revised form, June 12, 2020 Published, Papers in Press, June 17, 2020, DOI 10.1074/jbc.RA120.013589

Ellen K. Okuda[1], Fernando A. Gonzales-Zubiate[1], Olivier Gadal[2], and Carla C. Oliveira[1,*]

From the [1]Department of Biochemistry, Institute of Chemistry, University of São Paulo, São Paulo, Brazil and the [2]Laboratoire de Biologie Moléculaire Eucaryote, Centre de Biologie Intégrative (CBI), Université de Toulouse, CNRS, UPS, Toulouse, France

Edited by Craig E. Cameron

The RNA exosome is a multisubunit protein complex involved in RNA surveillance of all classes of RNA, and is essential for pre-rRNA processing. The exosome is conserved throughout evolution, present in archaea and eukaryotes from yeast to humans, where it localizes to the nucleus and cytoplasm. The catalytically active subunit Rrp44/Dis3 of the exosome in budding yeast (*Saccharomyces cerevisiae*) is considered a protein present in these two subcellular compartments, and here we report that it not only localizes mainly to the nucleus, but is concentrated in the nucleolus, where the early pre-rRNA processing reactions take place. Moreover, we show by confocal microscopy analysis that the core exosome subunits Rrp41 and Rrp43 also localize largely to the nucleus and strongly accumulate in the nucleolus. These results shown here shed additional light on the localization of the yeast exosome and have implications regarding the main function of this RNase complex, which seems to be primarily in early pre-rRNA processing and surveillance.

The RNA exosome is a protein complex that participates in processing and degradation of all classes of RNA in eukaryotes (1, 2). In *Saccharomyces cerevisiae*, the exosome is composed of a nine-subunit core (Exo9) that contains a heterohexameric ring formed by the subunits Rrp41, Rrp42, Rrp43, Rrp45, Rrp46, and Mtr3, and a heterotrimeric "cap" formed by the subunits Rrp4, Rrp40, and Csl4. Although the structure of the exosome core is conserved from archaea to eukaryotes, it has no catalytic activity in the latter (3). In yeast, Exo9 interacts with Rrp44/Dis3 in the nucleus and cytoplasm to form a 10-subunit complex (Exo10). Rrp44 is an RNase II family member, and has two catalytic sites, one with endoribonucleolytic activity (PIN) and a second with processive 3′-to-5′ exoribonucleolytic activity (RNB) (4–6). In yeast, the nuclear exosome contains Rrp6 (forming Exo11), an extra catalytic subunit with a distributive 3′-to-5′ exoribonuclease activity that binds to the trimeric cap and upper portion of the hexameric ring, opposite to the Rrp44-binding site. Rrp6 is the only nonessential exosome subunit, although the deletion of its gene results in a slow growth phenotype, temperature sensitivity, filamentous growth, and RNA processing defects (7–12).

Ribosome biogenesis involves the coordinated transcription, surveillance, modification, and processing of precursor rRNAs, which undergo modifications and several exo- and endonucleolytic cleavage reactions during its maturation process (13, 14). In the canonical pre-rRNA maturation pathway, the RNA exosome complex is responsible for the degradation of the spacer sequence 5′-ETS after cleavage at A_0, and for the 3′-5′ end processing of 7S pre-rRNA to the mature 5.8S rRNA (Fig. S1*A*) (8, 15). The 5′-ETS is released co-transcriptionally and completely degraded by the exosome, while SSU processome is formed by association of U3 snoRNP and other factors to the pre-rRNA being transcribed (16). Later during pre-rRNA processing, endonucleolytic cleavage at the C2 site in ITS2 of pre-rRNA 27S separates pre-rRNAs 7S (5.8S + 5′ region of ITS2) and 26S (3′ region of ITS2 plus 25S) (17), which undergo exonucleolytic processing by the exosome and Rat1/Rai1, respectively, to generate mature rRNAs 5.8S and 25S (17, 18). Mtr4 and the RNA exosome are essential for the ITS2 processing of 7S after cleavage at C2 (18), when the exosome subunit Rrp44 shortens 7S to the intermediate 5.8S + 30, which is then handed over to Rrp6 that trims it to 6S pre-rRNA, which gives rise to the mature 5.8S rRNA after further processing in the cytoplasm (19). Exosome is also involved in quality control steps of rRNA processing, targeting 23S rRNA generated by direct cleavage at the A3 site for degradation, and unprocessed ^{35}S rRNA (Fig. S1*B*) (20–22). Interestingly, despite the direct involvement of the exosome in 7S pre-rRNA processing and quality control, 60S subunits bearing 7S have been identified in polysomes of exosome cofactors mutants (23).

Although the structure and function of the exosome has been extensively studied in recent years, detailed information on the mechanisms responsible for the subcellular localization of its different forms is still lacking. Despite the identification of some of the yeast exosome subunits in the nucleolus (24), the core subunits of this complex are regarded as mainly present in nucleus and cytoplasm (3, 9, 24, 25). Rrp4 and Rrp6 have been reported to be present in nucleus and nucleolus, in addition to the cytoplasm in the case of Rrp4 (9). We have recently identified the nuclear import mechanisms for Rrp6 and shown that this exclusively nuclear subunit has multiple transport pathways, being bound by the α-importin Srp1 and β-importins Kap95 and Sxm1 (12). To gather more information on the transport of the exosome to the nucleus, we investigated the nuclear import pathway of the other exosome catalytically

This article contains supporting information.

* For correspondence: Carla C. Oliveira, ccoliv@iq.usp.br.

Present address for Fernando A. Gonzales-Zubiate: School of Biological Sciences and Engineering, Yachay Tech University, Ecuador.

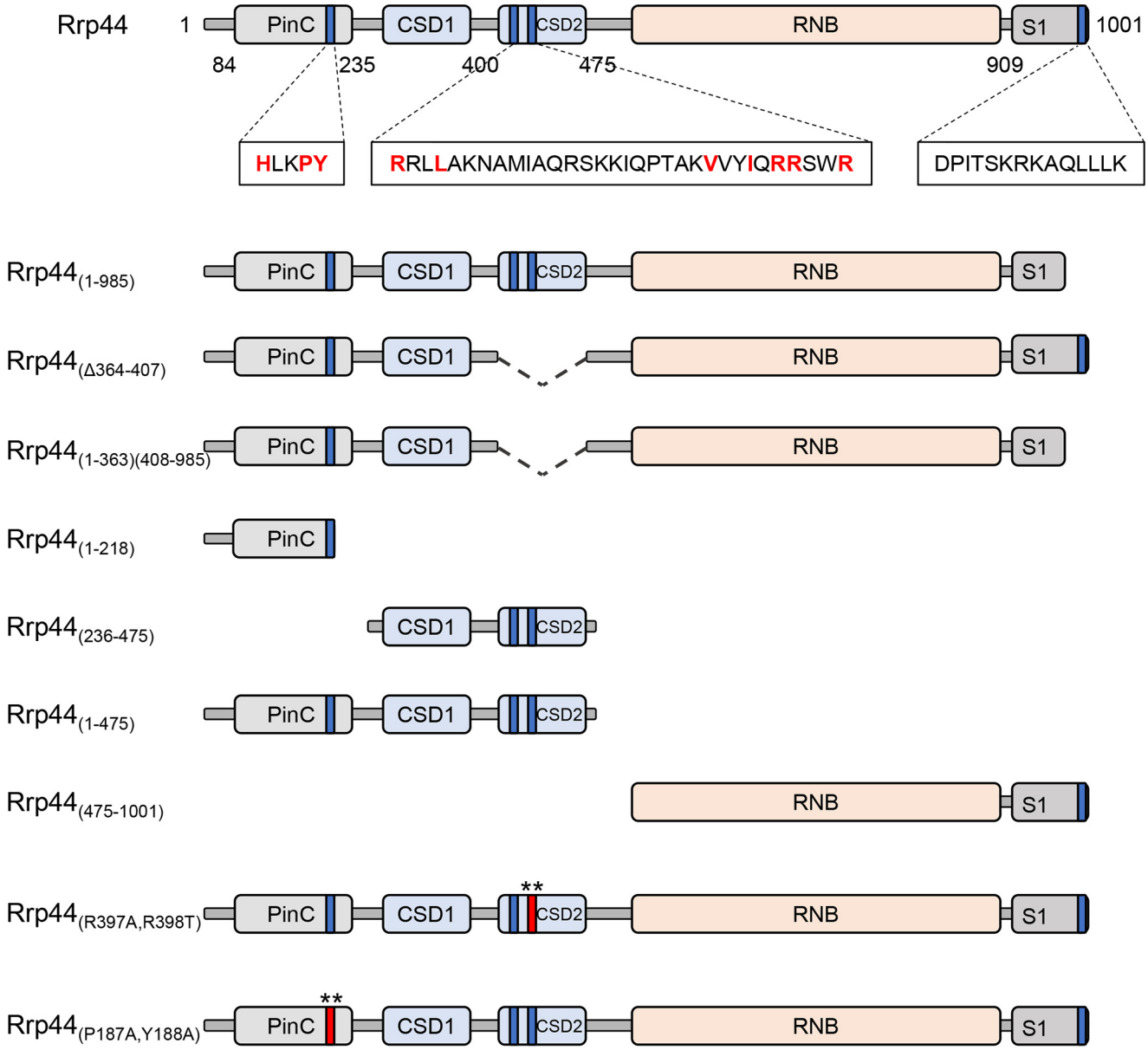

Figure 1. Schematic representation of the deletion and point mutants of Rrp44. Structural and catalytic domains of Rrp44 are shown. Positions of putative NLS are shown in *blue* and their sequences are highlighted. *Asterisks* over NLS in *red* indicate the positions of the point mutations.

active subunit, Rrp44, and show here that importins Srp1 (α) and Kap95 (β), respectively, are responsible for this transport, which occurs independently of Rrp6. Furthermore, we show that the exosome complex is highly concentrated in the nucleus, and more specifically in the nucleolus, where pre-rRNA is transcribed and where the early processing reactions take place.

Results

One of the essential functions of the exosome in yeast is the processing of pre-rRNA in the nucleus, which underlines the relevance of uncovering the mechanism of nuclear import that allows this protein complex to enter the nucleus. We have previously shown that one of the exosome active subunits, Rrp6, is transported to the nucleus by the karyopherins Srp1/Kap95 or Sxm1 (12), but information on the other catalytically active exosome subunit, Rrp44/Dis3, nuclear transport is lacking. Rrp44 has five distinct structural domains: an endonuclease PinC N-terminal domain, two CSD cold shock domains, an essential exoribonuclease domain, RNB, and an RNA-binding domain S1 (6). Based on software analyses (see "Experimental procedures"), we identified the presence of three putative nuclear localization signals (NLSs) in the amino acidic sequence of Rrp44 (named here NLS1, NLS2, and NLS3), each overlapping one of the functional domains, PinC, CSD2, and S1, respectively (Fig. 1).

NLS1 is a nuclear localization signal known as the PY-NLS, located in the PinC domain of Rrp44 between residues 172 and 188 (^{172}**RAIRK**TCQWYSE**H**LK**PY**^{188}). A weak consensus motif composed of an N-terminal hydrophobic or basic motif and a C-terminal R/H/K$X_{2\text{-}5}$PY recognized by importins Kap104, Sxm1/Kap108, Kap121, Kap114, Nmd5/Kap119, and Kap95 (26–28).

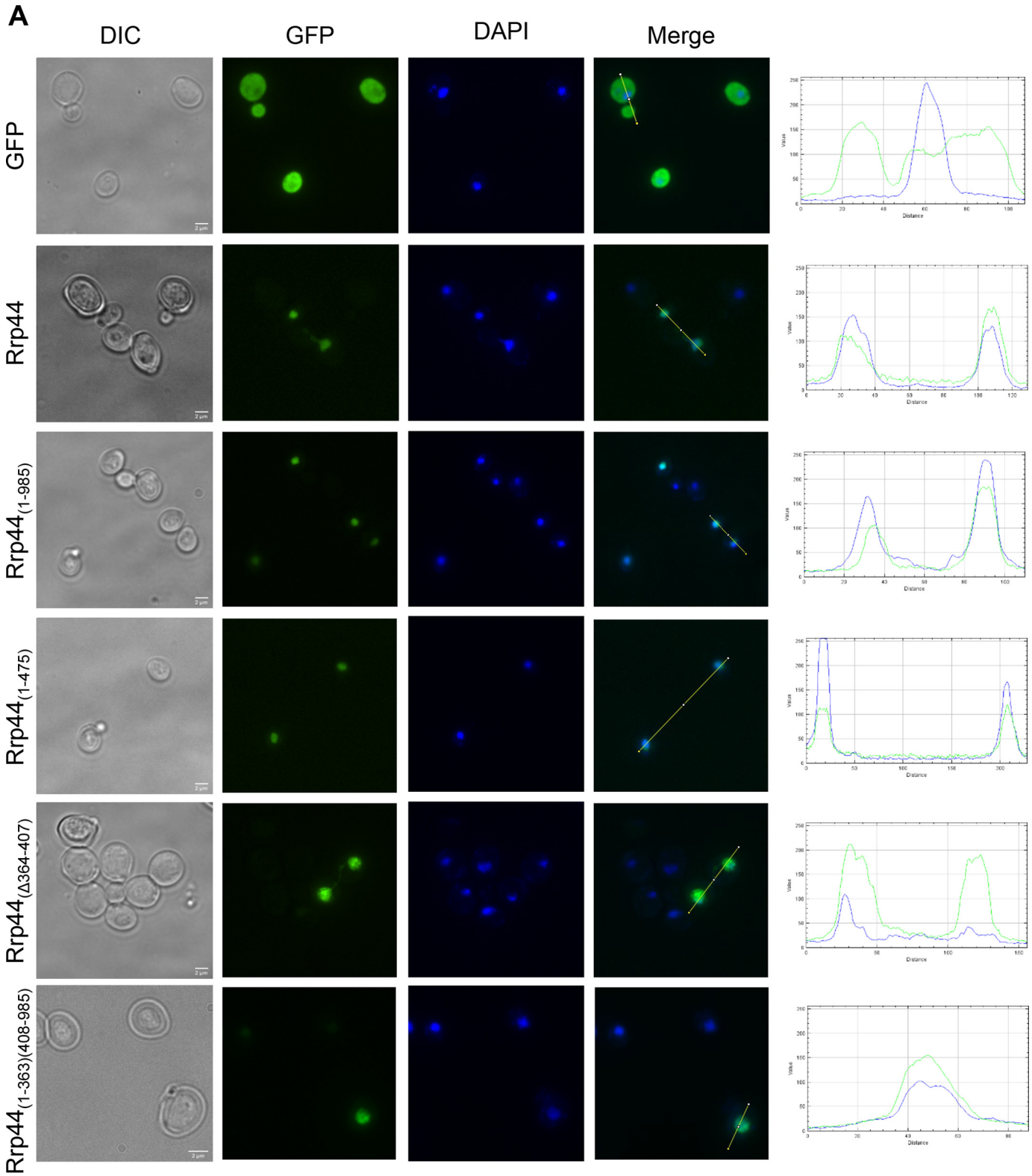

Figure 2. NLS1 is the most important region for Rrp44 nuclear import. Fluorescence microscopy images show the subcellular localization of the Rrp44 mutants expressed in WT cells. *A,* GFP, GFP-Rrp44, $Rrp44_{1\text{-}985}$, $Rrp44_{1\text{-}475}$, $Rrp44_{\Delta 364\text{-}407}$, and $Rrp44_{(1\text{-}363)(408\text{-}985)}$. *B,* $Rrp44_{1\text{-}218}$, $Rrp44_{236\text{-}475}$, $Rrp44_{475\text{-}1001}$, $Rrp44_{R397A,R398A}$, and $Rrp44_{P187A,\ Y188A}$. Analysis of GFP-Rrp44 relative to DAPI using ImageJ is shown on the *right*. Cells expressing $Rrp44_{1\text{-}218}$ show two phenotypes, both depicted here, with this mutant localized to the nucleus of 67% of cells, and present in aggregates in 30% of cells. GFP-Rrp44 relative to DAPI by using ImageJ is shown on the *right*. *Green lines* represent GFP and *blue lines* represent DAPI. Images were acquired and edited separately. Quantification of different phenotypes is shown in Fig. S3.

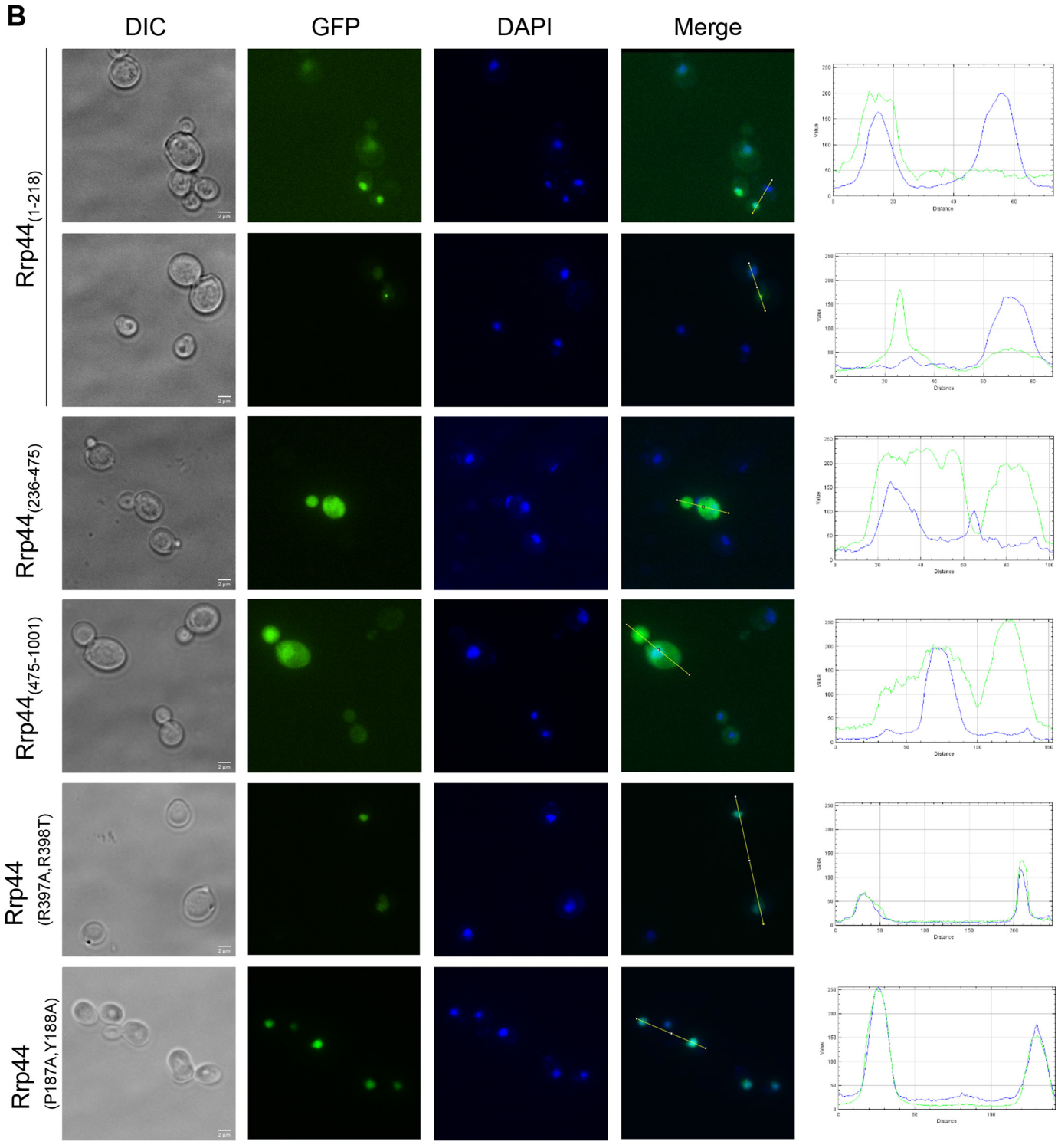

Figure 2—continued

NLS2 is located in the CSD2 domain between residues 370 and 401 (^{370}**R**RL**L**AKDAMIAQRSKKIQPTAK**V**VYI**Q**R**R**SW**R**^{401}) and contains the consensus NLS, R/KX_2LX_nV/YX_2V/IXK/RX_3K/R, recognized by the importins Kap114, Kap95, Kap123, Pse1, and Kap104 (29). NLS3 is located at the C terminus of Rrp44 between residues 988 and 1001 (^{988}DPITSKRKAELLLK^{1001}). The prediction of this NLS is based on its similarity to the *Drosophila* Rrp44 (dDis3), which is recognized by importin α3 (30, 31). These findings suggest that Rrp44 could be transported to the nucleus independently of other exosome subunits.

NLS1 is essential for nuclear import

To explore the importance of each of Rrp44 NLSs for its nuclear import, we constructed plasmids for episomal expression

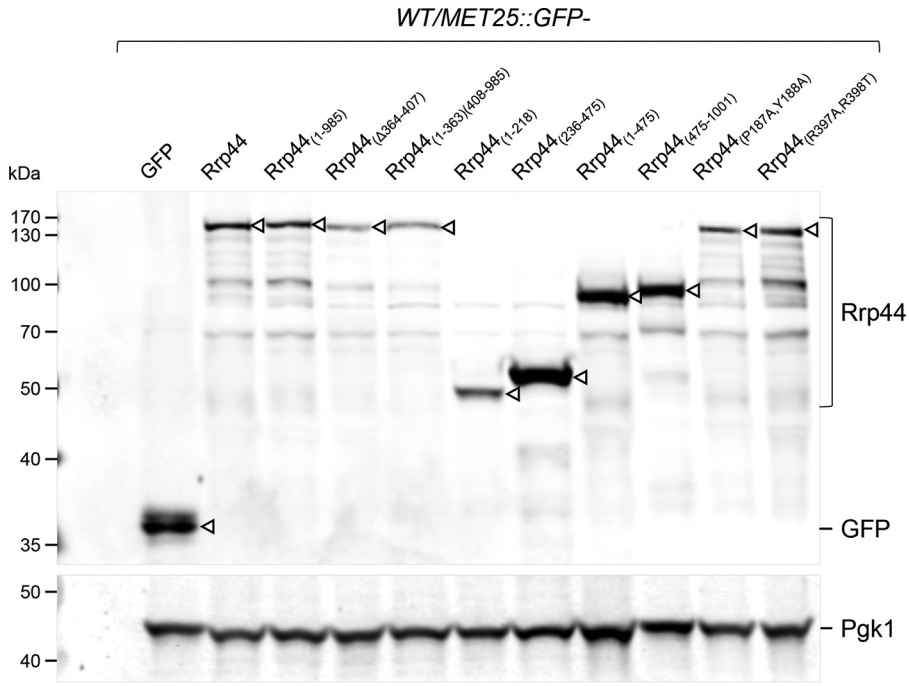

Figure 3. Expression of episomal Rrp44 mutants in WT cells. Western blotting for the determination of the expression levels of the GFP-Rrp44 mutants in BY4742 strain. Total cell extracts were separated by SDS-PAGE and subjected to Western blotting with antibodies against GFP and Pgk1, used here as an internal control. *Arrowheads* indicate the positions of the respective bands. In this 10% acrylamide gel, deletion mutants Rrp44$_{\Delta 364\text{-}407}$ and Rrp44$_{(1\text{-}363)(408\text{-}985)}$ run similar to full-length Rrp44. The 8% gel is shown in Fig. S4*A*.

of mutant versions of Rrp44 (Fig. 1). Rrp44 variants were fused to GFP at the N terminus and expressed under control of the *MET25* promoter, strongly induced in the absence of methionine. Analysis of the subcellular localization by fluorescence microscopy shows that despite being considered a nuclear and cytoplasmic protein (5, 32), full-length GFP-Rrp44 was found mainly concentrated in the nucleus (Fig. 2*A*), in agreement with high-throughput analyses (24).

Analysis of the subcellular localization of Rrp44 deletion and point mutants showed a variety of phenotypes depending on the presence of any of the putative NLS described above. Rrp44 mutants containing NLS1 in their sequence localized exclusively to the nucleus (Rrp44$_{1\text{-}985}$, Rrp44$_{1\text{-}475}$, Rrp44$_{R397A,R398T}$, Rrp44$_{P187A,Y188A}$) or concentrated in the nucleus, but were also present in the cytoplasm (Rrp44$_{\Delta 364\text{-}407}$, Rrp44$_{(1\text{-}363)(408\text{-}985)}$, and Rrp44$_{1\text{-}218}$) (Fig. 2). Mutant Rrp44$_{1\text{-}218}$ displayed two distinct phenotypes, some of the cells showed the protein concentrated in the nucleus, whereas others showed small cytoplasmic foci, which could correspond to degradation sites (Fig. 2*B*, Fig. S2). Despite the point mutations in PY-NLS, mutant Rrp44$_{P187A,Y188A}$ still concentrates in the nucleus, indicating that the remaining sequence suffices for importin recognition. Mutants lacking NLS1, although present in the nucleus, showed strong signals in the cytoplasm (Rrp44$_{236\text{-}475}$, Rrp44$_{475\text{-}1001}$). Mutant Rrp44$_{236\text{-}475}$, which contains only NLS2, showed the same phenotype as GFP alone, whereas Rrp44$_{475\text{-}1001}$ was present in cytoplasm, but concentrated in the nucleus in some cells (Fig. 2*B*).

Mutants lacking NLS2, Rrp44$_{\Delta 364\text{-}407}$, and Rrp44$_{(1\text{-}363)(408\text{-}985)}$ localized to the nucleus, which could suggest that NLS2 is not important for Rrp44 nuclear import. However, despite being concentrated in the nucleus, these mutants showed detectable signals in the cytoplasm (Fig. 2*A*), leading to the suggestion that in the absence of NLS2, Rrp44 is still transported to the nucleus but not very efficiently. Absence of the C-terminal NLS3, on the other hand, does not affect Rrp44 nuclear localization, because both mutants, Rrp44$_{1\text{-}985}$ and Rrp44$_{1\text{-}475}$, which lack NLS3, localized exclusively to the nucleus, and Rrp44$_{(1\text{-}363)(408\text{-}985)}$, which lacks NLS2 and NLS3, was concentrated in the nucleus (Fig. 2*A*).

Based on these results showing that deletion mutants containing NLS1 localize to the nucleus, whereas mutants lacking NLS1 are present in nucleus and cytoplasm (Fig. 2, Fig. S3), we can conclude that the presence of NLS1 plus either NLS2 or NLS3 is sufficient for Rrp44 nuclear localization. Hence, NLS1 would be the most important signal for Rrp44 nuclear import.

The expression of these deletion and point mutants of Rrp44 was analyzed by Western blotting of total cell extracts, which shows that most of the mutants are expressed at similar levels in yeast, and the protein bands detected have the expected molecular masses (Fig. 3). The ability of these mutants to complement growth of Δ*rrp44/GAL::RRP44* cells was tested by expressing the GFP-fused Rrp44 mutants in this conditional strain, growing on galactose or glucose media (expression or depletion of Rrp44, respectively). Toxicity of GFP-Rrp44 variants was evaluated with the expression of WT Rrp44 (galactose) in the presence or absence of methionine for lowering or increasing the expression of the variants, respectively. The results show that point mutants Rrp44$_{R397A,R398T}$ (NLS2 mutant) and Rrp44$_{P187A,Y188A}$ (NLS1 mutant), which localize to the nucleus, fully complement growth of Δ*rrp44/GAL::RRP44* on glucose, similar to GFP-Rrp44 (Fig. 4). The deletion mutant

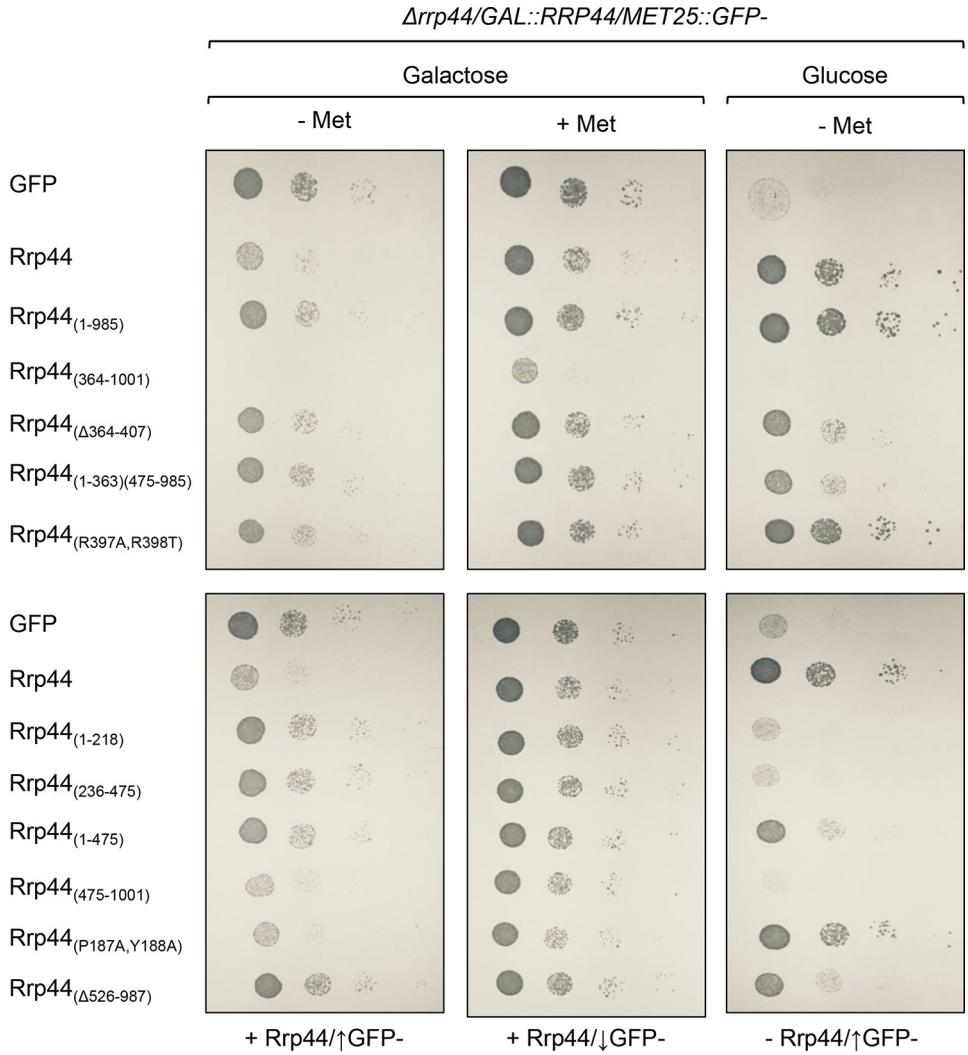

Figure 4. Analysis of growth of conditional strain Δ*rrp44/GAL::RRP44* expressing Rrp44 mutants. Conditional strain was transformed with plasmids containing the Rrp44 mutants under control of *MET25* promoter, and incubated in galactose (expression of WT Rrp44) or glucose (expression of Rrp44 mutants) medium, in the presence or absence of methionine (lower and higher levels of the mutants, respectively). Mutants $Rrp44_{\Delta 364\text{-}407}$ and $Rrp44_{(1\text{-}363)(408\text{-}985)}$ partially complement growth in glucose, whereas $Rrp44_{1\text{-}985}$, $Rrp44_{R397A,R398A}$, and $Rrp44_{P187A,Y188A}$ fully complement growth in glucose, although overexpression of the latter inhibits growth in galactose.

$Rrp44_{1\text{-}985}$, which lacks NLS3, but localizes to the nucleus, also complements growth. These results reinforce those presented above, that the Rrp44 mutants transported to the nucleus are functional. Confirming the results of protein localization, mutants $Rrp44_{\Delta 364\text{-}407}$ and $Rrp44_{(1\text{-}363)(408\text{-}985)}$ partially complement growth of Δ*rrp44/GAL::RRP44* on glucose. Despite being transported to the nucleus, mutants with further deletions in Rrp44 sequence, resulted in nonfunctional proteins (Fig. 4). Interestingly, co-expression of GFP-Rrp44 at high levels (Gal) and functional Rrp44 mutants (-Met) led to slow growth, contrary to what was seen on glucose (Fig. 4). Addition of methionine to the medium alleviates this effect, increasing growth. These results suggest that high levels of Rrp44, combined with high levels of GFP-Rrp44, are deleterious to the cells. Mutant $Rrp44_{364\text{-}1001}$, which showed dominant-negative effects, strongly inhibiting growth in all conditions, and displayed various localization phenotypes (Fig. 4 and data not shown), and mutant $Rrp44_{\Delta 526\text{-}987}$, which was not detected by Western blotting, were therefore not further analyzed.

These growth complementation results are consistent with the analysis of pre-rRNA processing on glucose, when GFP-tagged Rrp44 variants are expressed in the absence of WT Rrp44. As a control, rRNA processing was analyzed in the presence of WT Rrp44 (galactose). In the absence of Rrp44, 7S rRNA accumulates, without accumulation of detectable 5.8S + 30 species. In the absence of Rrp6, 7S processing by Rrp44 leads to strong accumulation of 5.8S + 30 rRNA (detected with both probes P1 and P2). Point mutants $Rrp44_{P187A,Y188A}$ and $Rrp44_{R397A,R398T}$ fully complement the depletion of WT Rrp44, visualized by the efficient processing of 7S pre-rRNA and formation of mature 5.8S rRNA (Fig. 5 and Fig. S9). Expression of the mutants $Rrp44_{1\text{-}218}$ (PIN domain), $Rrp44_{236\text{-}475}$ (CSD1 + CSD2), or $Rrp44_{1\text{-}475}$ (PIN + CSD1 + CSD2) leads to processing defects, with accumulation of pre-rRNA 7S and consequent decreased levels of mature 5.8S rRNA. Interestingly, mutant $Rrp44_{1\text{-}475}$ accumulates at low level and intermediate very similar to 5.8S + 30, which is a characteristic of strains lacking Rrp6 (Fig. 5). Note that such rRNA species are better detected with

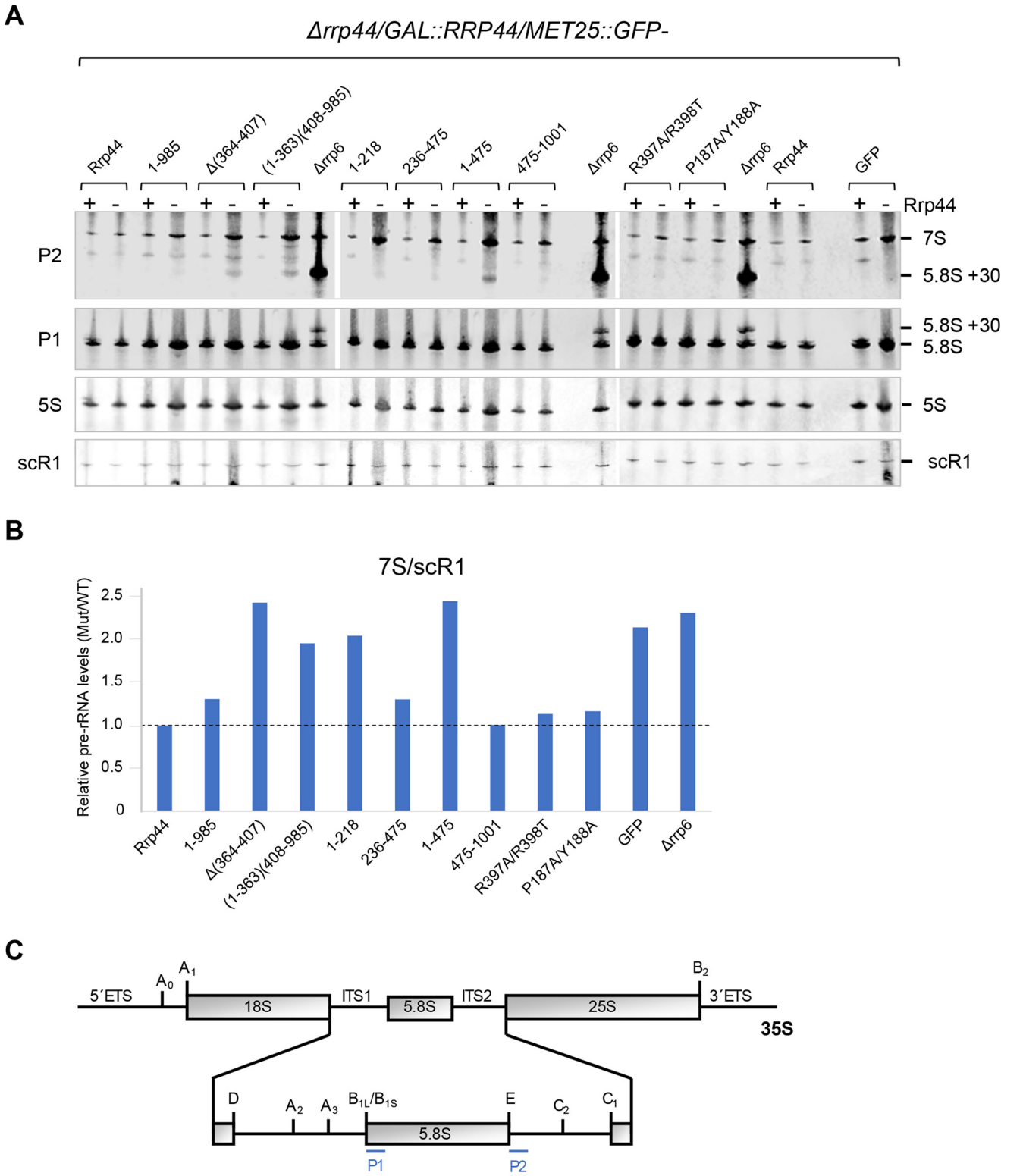

Figure 5. Analysis pre-rRNA processing in Rrp44 mutants. Northern hybridization of total RNA extracted from *Δrrp44/GAL::RRP44/MET25::GFP*$^{-}$ strains growing either in galactose (+ WT Rrp44) or glucose (−WT Rrp44) medium, and separated by electrophoresis on denaturing polyacrylamide gels. Precursor and mature rRNAs detected with the different probes are indicated on the *right*. 5S rRNA and scR1 were used as controls of RNAs not processed by the exosome. A representative of three independent experiments is shown. *B,* quantification of the bands detected by Northern hybridization. Signals of pre-rRNA 7S were corrected for scR1 signals and the plot shows the levels or 7S in the mutants relative to Rrp44 growing in glucose. *C,* schematic representation of the yeast ^{35}S pre-rRNA indicating the hybridizing positions of the probes.

P2, which hybridizes to the ITS2 region. In addition to 5.8S + 30, mutants Rrp44$_{\Delta 364\text{-}407}$ and Rrp44$_{(1\text{-}363)(408\text{-}985)}$ also accumulate intermediates longer than 5.8S + 30 (Fig. 5). Mutant Rrp44$_{475\text{-}1001}$ (RNB + S1 domains), on the other hand, shows lower levels of pre-rRNA 7S and mature 5.8S (Fig. 5). These results suggest that Rrp44$_{475\text{-}1001}$ may not associate stably with

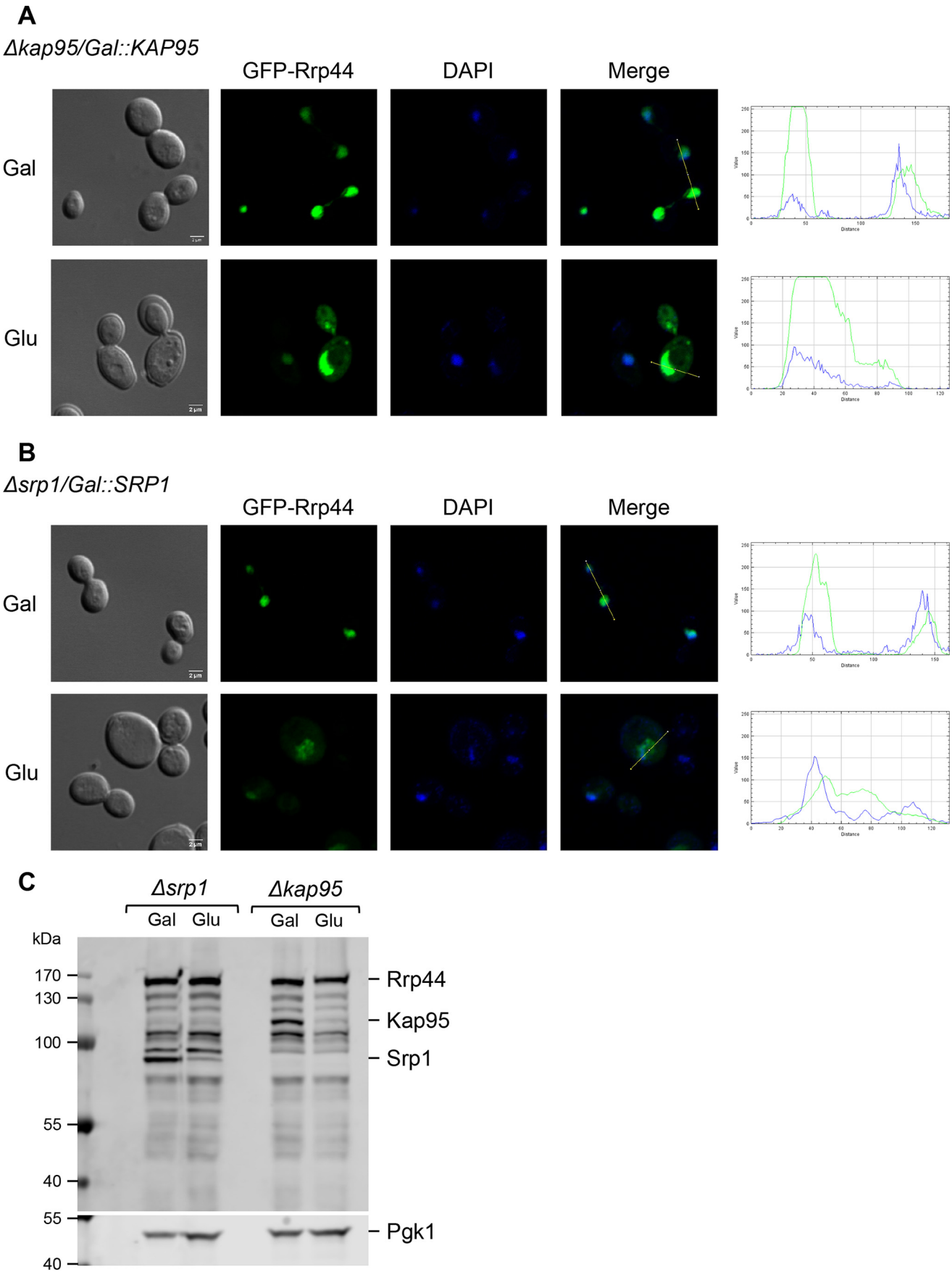
A
Δkap95/Gal::KAP95
GFP-Rrp44
DAPI
Merge
Gal
Glu
B
Δsrp1/Gal::SRP1
GFP-Rrp44
DAPI
Merge
Gal
Glu
C
Δsrp1
Δkap95
Gal
Glu
Gal
Glu
kDa
170
130
100
55
40
55
40
Rrp44
Kap95
Srp1
Pgk1

the exosome core, decreasing the efficiency of 7S processing, but may be free to degrade RNAs, leading to the decreased levels of both precursor and mature rRNAs. An overview of the phenotypes of the Rrp44 mutants relative to WT is shown in Fig. S5.

Rrp44 is transported to the nucleus by karyopherins Kap95 and Srp1

To better understand the nuclear import pathway of Rrp44 and identify the karyopherins involved in this process, GFP-Rrp44 was expressed in strains with mutated karyopherin genes, chosen based on the putative NLSs present in the Rrp44 sequence. Deletion mutants of the nonessential karyopherins Sxm1, Kap123, and Kap114 were transformed with a plasmid coding for GFP-Rrp44 and subcellular localization of this protein was analyzed by fluorescence and confocal microscopy. The results show that none of these karyopherins affects Rrp44 localization (Fig. S6 and data not shown). Lowering levels of Srp1 or Kap95 by incubating strains Δ*srp1/GAL::SRP1* and Δ*kap95/GAL::KAP95* on glucose medium, on the other hand, strongly affects GFP-Rrp44 localization, leading to partial mislocalization of this protein to the cytoplasm, despite still being concentrated in the nucleus (Fig. 6). These results indicate that Kap95 and Srp1 are the main karyopherins involved in nuclear import of Rrp44.

Because Srp1 and Kap95 affected Rrp44 localization, physical interaction between these proteins was analyzed by co-immunoprecipitation after expression of GFP-Rrp44 and protein A-tagged karyopherins in yeast. The results show that both A-Srp1 and A-Kap95 co-immunoprecipitate GFP-Rrp44 (Fig. 7*A*), confirming the interaction between these proteins and the involvement of Srp1 and Kap95 in the nuclear transport of Rrp44. Because the GFP tag alone was also detectable in the elution fractions, to exclude that interaction was due to GFP, an additional experiment was performed, in which extracts from yeast cells expressing GFP or GFP-Rrp44 were incubated with IgG-Sepharose without previous incubation with the karyopherins. After extensive washing, eluted proteins were analyzed by Western blotting, which shows that GFP binds unspecifically the resin with much higher affinity than GFP-Rrp44 (Fig. S4*B*), accounting for the background binding detected in the co-immunoprecipitation experiments (Fig. 7*A*). These results are in agreement with global protein interaction data that indicated protein complexes containing both Rrp44 and Srp1 (33, 34).

To determine whether Srp1 and Kap95 were capable of interacting directly with Rrp44 *in vitro*, protein pulldown assays were performed. Recombinant GST-Rrp44 was immobilized on GSH-Sepharose beads and then incubated with His-Kap95 or His-Srp1. Fractions were separated by SDS-PAGE and subjected to Western blotting with antibodies against the His and GST tags. The results show the direct interaction between GST-Rrp44 and His-Kap95 (Fig. 7*B*). Although His-Kap95 is also pulled down with GST, it binds GST-Rrp44 more efficiently, as indicated by the intensity of the bands detected in elution fractions. His-Srp1, however, was not detected in the elution (Fig. 7*B*, *lower panel*). These results suggest that Kap95 binds Rrp44 NLS, being responsible for its nuclear transport. Srp1 may indirectly interact with Rrp44, depending on β-importins such as Kap95 to recognize this cargo protein. Combined, the results shown here strongly indicate that Rrp44 is transported to the nucleus by a Kap95-dependent import pathway, either by itself, complexed with Srp1, or with another β-karyopherin.

Nuclear transport of the exosome complex

Although Rrp6 has been shown to have multiple NLS and transport pathways (12), it is generally not considered to be responsible for the nuclear import of other exosome subunits because it is not an essential yeast protein. The lack of effect of Rrp6 on nuclear transport of core exosome subunits was confirmed here upon analysis of subcellular localization of Rrp44, Rrp41, and Rrp43 in Δ*rrp6* cells (Fig. S7). Upon identifying NLS in Rrp44, we analyzed whether this essential exosome subunit influences the nuclear import of other exosome subunits. The episomal GFP-fused exosome subunits Rrp6, Rrp41, and Rrp43 were expressed in Δ*rrp44/GAL::RRP44* either in the presence (Gal) or upon depletion of Rrp44 (Glu). Contrary to Rrp6 and Rrp44, Rrp41 and Rrp43, expressed under the strong *MET25* promoter, are present in both nucleus and cytoplasm. Depletion of Rrp44 does not significantly affect the localization of these exosome subunits (Fig. 8), suggesting independent nuclear transport pathways. The nonaffected GFP-Rrp6 localization in the absence of Rrp44 was expected given the already described nuclear import pathways of Rrp6 (12). Control experiments in WT cells confirm that when overexpressed using episomal genes under control of *MET25* promoter, Rrp41 and Rrp43 localize to the nucleus and cytoplasm (Fig. S8). Overexpressed Rrp44 and Rrp6, on the other hand, show nuclear localization (Fig. S8).

Exosome subcellular localization

Curiously, as shown here, Rrp44 is mainly nuclear, whereas the exosome RNase PH ring subunits Rrp41 and Rrp43 show a nuclear and cytoplasmic localization. To determine whether this phenotype is due to the overexpression of the exosome subunits coded in multicopy plasmid under control of the strong *MET25* promoter, chromosomal C terminally tagged GFP-fused exosome subunits genes, under control of their endogenous promoters, were constructed for Rrp44, Rrp6, Rrp41, and Rrp43. No growth defect was observed, showing that C terminally tagged proteins expressed at endogenous levels remain functional. Although the subunits of Exo10 are considered to be present both in nucleus and cytoplasm (9), the results shown

Figure 6. Inhibition of karyopherins expression affects the subcellular localization of GFP-Rrp44. *A,* laser scanning confocal microscope images show the subcellular localization of GFP-Rrp44 after inhibition of Kap95 expression in glucose medium in Δ*kap95/GAL::KAP95* cells. GFP-Rrp44 relative to DAPI by using ImageJ is shown on the *right*. *Green lines* represent GFP and *blue lines* represent DAPI. *B,* analysis of the subcellular localization of GFP-Rrp44 after inhibition of Srp1 expression in glucose medium in Δ*srp1/GAL::SRP1* cells. GFP-Rrp44 relative to DAPI is shown on the *right*. *C,* Western blotting showing the repressed expression of the karyopherins in glucose medium.

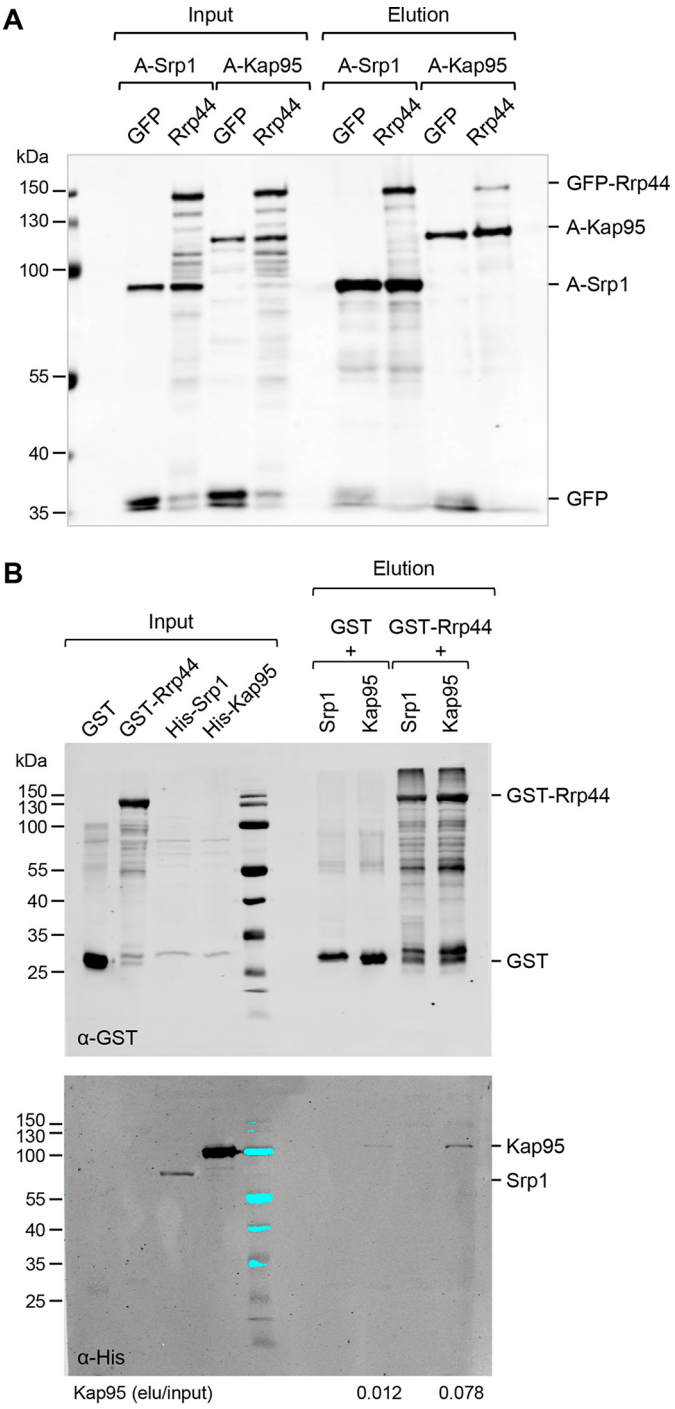

Figure 7. Interaction of Rrp44 with karyopherins. *A,* GFP-Rrp44 co-immunoprecipitates with A-Srp1 and A-Kap95. Yeast strains expressing ProtA-Srp1 or ProtA-Kap95, and GFP or GFP-Rrp44 were used in co- immunoprecipitation experiments. ProtA-Kap95 and ProtA-Srp1 were immobilized on IgG-Sepharose beads, and co-immunoprecipitated proteins were analyzed by Western blotting with antibody against GFP. Input and elution fractions are shown. GFP-Rrp44 is co-immunoprecipitated with both karyopherins. *B,* GST-Rrp44 pulls down His-Kap95. *E. coli* expressed GST and GST-Rrp44 bound to GSH-Sepharose beads were incubated with His-Srp1, or His-Kap95-containing extracts. After washing, bound proteins were eluted with GSH and analyzed by Western blotting. *Numbers below* indicate the quantification of the Kap95 signal in the elution fractions relative to the input. The same membrane was incubated with antibodies against GST and His tags. Saturated marker signals appear as *bluish bands* at 800 nm (*lower panel*). The figure shown is representative of three independent experiments.

here demonstrate that core subunits Rrp41 and Rrp43, and the catalytically active subunits Rrp44 and Rrp6 are all concentrated in the nucleus (Fig. 9). These proteins expressed at endogenous levels are visible almost exclusively in the nucleus, and more strikingly, are concentrated in the nucleolus (Fig. 9). Importantly, analyses using confocal microscopy and quantification of the sum of fluorescent signal, followed by projection along the *z* axis of all acquired confocal images and calculation of enrichment of the exosome signal in each cellular compartment (see "Experimental procedures"), corroborates the nucleolar localization of the exosome. Exosome concentration in the nucleoplasm is 6 to 9 times higher than in the cytoplasm, whereas nucleolar exosome concentration is 10 to 20 times higher than in the cytoplasm (Fig. 9). Quantification of the signal of these exosome subunits in each of the subcellular compartments (nucleolus, nucleus and cytoplasm) relative to the total signal in the cells shows that 70–80% of the exosome signal is in the nucleus (Fig. S10).

Careful inspection of individual *z* sections of the acquired fluorescent images, however, shows that despite being concentrated in the nucleolus, exosome subunits localization is slightly different from that of RNA polymerase I (Rpa190), as if in a different subnucleolar compartment (Fig. 10). These results strongly suggest that in the nucleolus, nascent rRNAs are exposed to a high concentration of exosome in a "processing compartment" adjacent, but distinct from RNA polymerase I, for processing and quality control of pre-rRNAs.

Discussion

The RNA exosome was first identified in *S. cerevisiae* as an RNase involved in maturation and quality control of stable RNAs (8, 15). In the subsequent studies, it became clear that the exosome is a protein complex conserved throughout evolution, which is present in the nucleus and cytoplasm of eukaryotic cells, where it interacts with many cofactors and participates in different RNA processing and degradation pathways (3, 35, 36).

In yeast, Exo10, composed of the exosome core and Rrp44, is considered to be present both in nucleus and cytoplasm, participating in different reactions in each of these subcellular compartments (32). We have previously identified the nuclear import pathways of Rrp6 and shown that this nuclear exosome subunit has redundant mechanisms of transport to the nucleus, directly interacting with α-importin Srp1 and β-importins Kap95 and Sxm1 (12). To better understand the mechanism of exosome assembly and transport to the nucleus, where this complex participates in the essential process of ribosome maturation, we investigated here the nuclear import pathway of the other catalytically active exosome subunit, Rrp44.

We identified three putative NLSs in the primary sequence of Rrp44 and constructed deletion and point mutants to determine the Rrp44 sequences mediating its transport to the nucleus. We show evidence that NLS1 is the most important sequence, but not the only NLS, for the nuclear import of Rrp44, which suggests that different karyopherins may bind Rrp44 for directing it to the nucleus. Depletion of Kap95 strongly affects the nuclear localization of Rrp44, and accordingly, NLS1

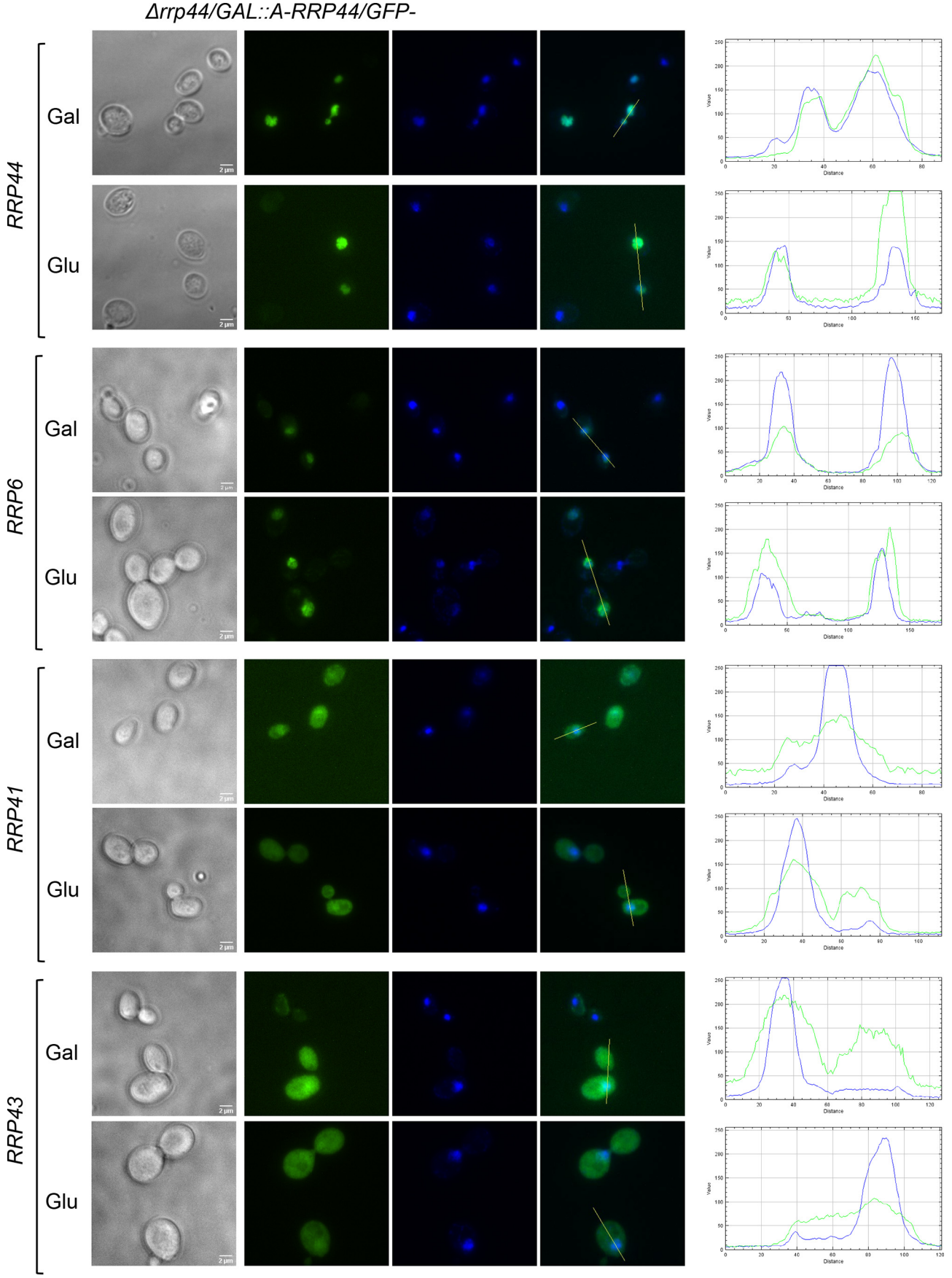
Δrrp44/GAL::A-RRP44/GFP-
RRP44
Gal
Glu
RRP6
Gal
Glu
RRP41
Gal
Glu
RRP43
Gal
Glu
Value
Distance

contains the consensus sequence for Kap95 binding, a PY-NLS (37). However, point mutant $Rrp44_{P187A,Y188A}$ still localizes to the nucleus, suggesting that additional signals are recognized by Kap95. Although Srp1 also affects Rrp44 transport to the nucleus, a classical NLS was not found in the Rrp44 sequence, suggesting that Srp1 could recognize a nonconsensus NLS, or that the transport is mediated by the Kap95/Srp1 heterodimer upon recognition of the NLS by Kap95, or by an additional β-karyopherin.

Rrp44 has endo- and exonucleolytic activities (5, 38), and is involved in pre-rRNA processing in nucleus and nucleolus (8). The mutants that contain the exonuclease domain of Rrp44 and at least two of the putative NLSs, localize to the nucleus and complement growth of the Δ*rrp44/GAL::A-RRP44* strain. Analysis of pre-rRNA processing in the mutants show that the mutants that do not localize to the nucleus, or that do not contain the RNB domain, display a defective pre-rRNA processing phenotype, with accumulation of intermediates with sizes in the range between pre-rRNAs 7S and 5.8S + 30. Importantly, these intermediates are not substrates for Rrp6, which process the product of the Rrp44 reaction, 5.8S + 30 (7). The intermediates accumulating in the presence of nonfunctional Rrp44 mutants have longer extensions at the 3' end than 5.8S + 30, and have also been observed in mutants of core exosome subunits (8). Interestingly, mutant $Rrp44_{475\text{-}1001}$ (containing RNB + S1 domains, but lacking PIN and CSD domains) shows decreased levels of both precursor and mature rRNAs. These results are in agreement with Rrp44 structural data showing that PIN and CSD domains are responsible for the stable interaction between Rrp44 and the RNase PH ring of the exosome (39). Rrp44 lacking these domains may not associate stably with the exosome, decreasing the efficient processing of 7S, but instead, may be free and more active to degrade RNAs (40, 41).

As shown here, depletion of Rrp44 does not affect nuclear localization of Rrp6, as expected, given that Rrp6 has its own NLSs (12), and does not directly interact with Rrp44 (39, 41). Interestingly, depletion of Rrp44 does not affect localization of episomal core exosome subunits either, suggesting a different mechanism of transport for the remaining subunits of this complex.

The most striking results coming from the analyses described here are the very low concentration in the cytoplasm of all the exosome subunits analyzed. Exosome is not only concentrated in the nucleus, but specifically in the nucleolus. This information is relevant in light of the function of the yeast exosome. In the cytoplasm, the exosome participates in the minor pathway of mRNA decay, degrading 3'-5' deadenylated mRNAs (42–44). The major pathway of cytoplasmic mRNA degradation in yeast does not involve the exosome, and starts with deadenylation of mRNAs by the Ccr4-Not complex (42, 45, 46), followed by decapping by Dcp1 (47, 48) and 5'-3' degradation by Xrn1 (49, 50). Pre-rRNA processing and surveillance, on the other hand, starts in the nucleolus and continues to the nucleoplasm, as the pre-ribosomal particles are concomitantly transported toward the cytoplasm (51).

As soon as 5'-ETS is released after co-transcriptional cleavage of pre-rRNA at sites A_0-A_1, the exosome can degrade it in the nucleolus, after being recruited there by SSU processome factors (51–54). The results shown here reinforces the importance of the exosome for pre-rRNA processing and quality control, by showing that the exosome is mainly concentrated in the nucleolus. The concentration of the exosome in the nucleolus also corroborate recent data showing the interaction of exosome subunits with pre-ribosomal particles 90S, pre-40S, and pre-60S, interactions that were stabilized by the inhibition of pre-rRNA processing by the depletion of pre-60S factor Nop53 (55).

As we also show here, the nucleolar concentration of the exosome subunits can only be appreciated when the GFP-fused proteins are expressed at endogenous levels. Overexpression of these proteins in plasmid-based systems lead to the visualization of weak signals in the cytoplasm and very strong nuclear signals, overshadowing the nucleolus.

Not only were the exosome subunits concentrated in the nucleolus, but careful high-resolution analysis of protein localization showed that when compared to RNA polymerase I subunit Rpa190 on individual z sections of spinning disk confocal microscopy, the exosome subunits do not exactly overlap Rpa190, suggesting a slightly different localization. Interestingly, recent data on mammalian cells show that the box C/D snoRNP subunit fibrillarin, which is also part of the SSU processome, does not exactly colocalize with RPA194, but rather shows a phase separation between rRNA transcription and processing (56). Our results could suggest that transcribed rRNA is co-transcriptionally processed in an associated compartment containing the exosome.

In summary, here we show that the exosome catalytic subunit Rrp44 is transported to the nucleus independently of other subunits. Importantly, we show that the yeast exosome is concentrated in the nucleolus, in a subcompartment flanking but different from RNA polymerase I, placing the exosome in the early phases of pre-rRNA processing.

Experimental procedures

Construction of strains and yeast growth condition

Yeast maintenance and growth was performed in YPD medium (1% yeast extract, 2% peptone, and 2% glucose), or YNB medium (0.67% yeast nitrogen base, 0.5% $(NH_4)_2SO_4$, and 2% glucose or galactose) supplemented with the required amino acids. Plasmids constructed in this study, described in Table 1, were built according to standard cloning techniques and sequenced by the Big Dye method (PerkinElmer Life Sciences). Plasmids expressing the GFP fusions in yeast were constructed by inserting DNA fragments into pUG34 plasmid (57) using oligonucleotides with specific restriction sites

Figure 8. Depletion of Rrp44 does not affect subcellular localization of core exosome subunits Rrp41 and Rrp43. Δ*rrp44/GAL::RRP44* was transformed with plasmids expressing GFP-fused exosome subunits Rrp44, Rrp6, Rrp41, and Rrp43 and incubated in media containing either galactose (Rrp44 expression) or glucose (Rrp44 repression). All four exosome subunits are concentrated in the nucleus, although Rrp41 and Rrp43 are also visible in the cytoplasm. Images were acquired and edited separately. GFP-fused proteins relative to DAPI by using ImageJ is shown on the *right*. *Green lines* represent GFP and *blue lines* represent DAPI.

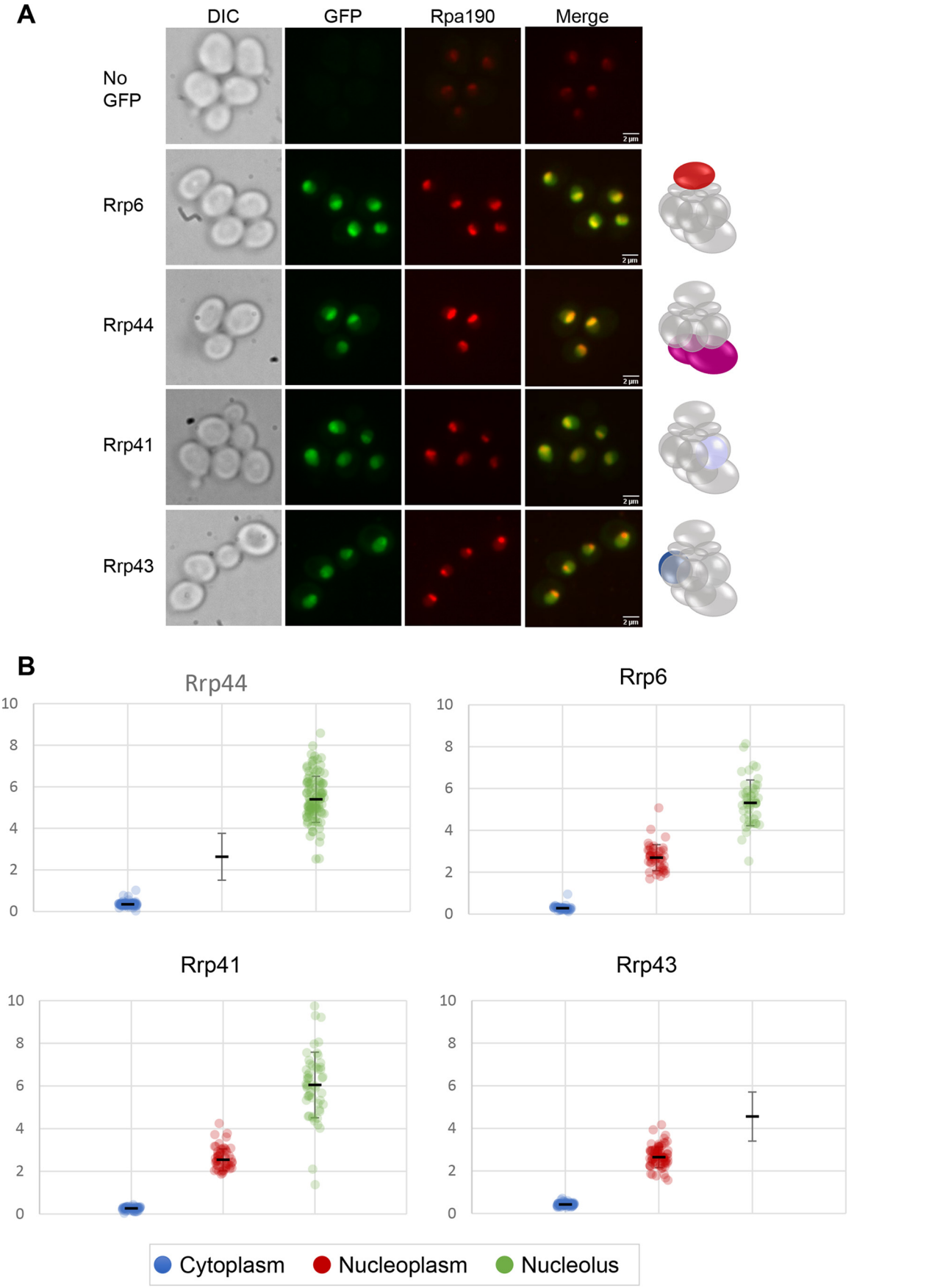
A
DIC
GFP
Rpa190
Merge
No GFP
Rrp6
Rrp44
Rrp41
Rrp43
2 μm
B
Rrp44
Rrp6
Rrp41
Rrp43
10
8
6
4
2
0
Cytoplasm
Nucleoplasm
Nucleolus

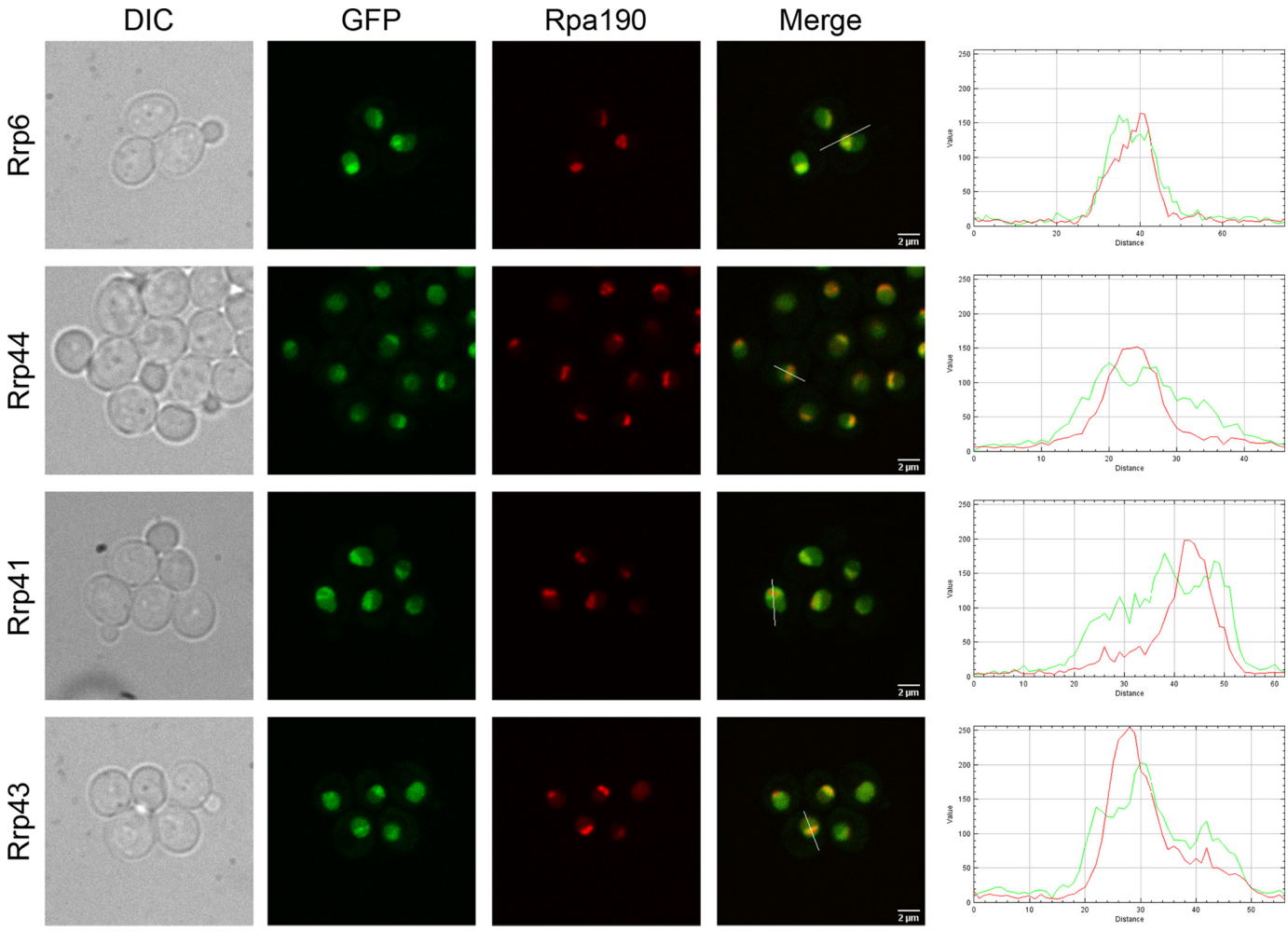

Figure 10. Exosome subunits do not co-localize exactly with nucleolar RNA polymerase I subunit Rpa190. GFP-tagged images obtained by Z section of spinning disk confocal microscope shows that exosome subunits have slightly different localization from Rpa190-mCherry, used as nucleolar marker. Note that single Z step images are different from Z-projected images, which shows the sum of all detected signal of cells.

(sequences available upon request). Expression of these GFP fusions was regulated by *MET25* promoter. Rrp44 point mutations were obtained by site-directed mutagenesis (Stratagene or In-Fusion-Takara) using plasmid pUG34-RRP44 as template and oligonucleotides containing the respective mutations. Plasmid pRS305-NUP57-tDimerRFP (58) was constructed as follows. NUP57 was amplified as two overlapping PCR fragments (primer pairs 1568/1570 and 1569/1571-matrix strain BY4741). The two PCR fragments were mixed and used as matrix with primers 1568/1571 to amplify full-length NUP57 with an internal BglII site. The NUP57-containing fragment was cloned in pRS305-NUP2-tDimerRFP (59) as a NotI-BamHI fragment. To construct a Nup57 *t*-dimer genomic-tagged strain, plasmid pRS305-Nup57-tDimer was linearized with BglII and inserted by homologous recombination in a BY4742 strain. It was selected for leucine prototrophy, and checked by fluorescence microscopy. Plasmid pFA6-mCherry-KlURA3 was constructed by cloning into pFA6-GST-KIURA3 PacI-Asc1 mCherry a fragment from pFA6-mCherry-HIS3.

Haploid strain Δ*rrp44/YCplac33-GAL::A-RRP44* was obtained after sporulation of the diploid strain *RRP44/*Δ*rrp44* previously transformed with plasmid YCplac33-GAL::A-RRP44 (Table 2). Strains bearing genomic insertion of GFP or mCherry were constructed by amplifying a PCR cassette containing the *URA3* gene from *Kluyveromyces lactis* as a selectable marker and GFP tag or mCherry tag sequence from plasmids pFA6-GFP(S65T)-KIURA3 or pFA6a-mCherry-KIURA3, respectively. The PCR fragment was inserted by homologous recombination downstream from each protein gene bearing a TAP-tag (60) using the Swap-tag method (61). Transformants were selected for uracil prototrophy and checked by PCR of the targeted

Figure 9. Endogenously expressed GFP-fused exosome subunits localize to the nucleolus. *A*, Z-projection of high resolution spinning-disk laser scanning confocal microscope images show the subcellular localization of GFP-tagged exosome subunits. Rpa190-mCherry was used as nucleolar marker. *B*, exosome subunits enrichment in different cell compartments. We calculated the enrichment of the GFP-tagged exosome subunits signals in each compartment over an homogeneous distribution of the cellular signal. For that, we calculated the mean intensity of each compartment and divided this value by the computed mean intensity (total cell signal/total cell surface). *Blue dots* represent cytoplasm enrichment, *red dots* represent nucleoplasm, and *green dots* represent nucleolus.

Table 1
Plasmids

Name	Characteristics/markers	Reference
pFA6-mCherry-HIS3	Used for cloning pFA6a-mCherry-KIURA3	67
pFA6-GST-KIURA3	Used for cloning pFA6a-mCherry-KIURA3	61
pFA6-GFP(S65T)-KIURA3	URA3, integrative, C-term GFP	61
pRS305-Nup2-tDimer	LEU2, integrative, Nup57-RFP	59
pRS305-Nup57-tDimer	LEU2, integrative, Nup57-RFP	58
pFA6a-mCherry-KIURA3	URA3, integrative, C-term mCherry	This work
pUN-GFP-Nop1	LEU2, CEN/ARS, GFP-NOP1	68
pUN100-mCherry-Nop1	LEU2, CEN/ARS, mCherry-NOP1	69
pUG34	HIS3, CEN/ARS, PMET25::yEGFP3	57
pUG34-Rrp6	HIS3, CEN/ARS, PMET25::yEGFP3-RRP6	12
pUG34-Rrp41	HIS3, CEN/ARS, PMET25::yEGFP3-RRP41	This work
pUG34-Rrp43	HIS3, CEN/ARS, PMET25::yEGFP3-RRP43	This work
pUG34-Rrp44	HIS3, CEN/ARS, PMET25::yEGFP3-RRP44	This work
pUG34-rrp44(1-985)	HIS3, CEN/ARS, PMET25::yEGFP3-rrp44(1-985)	This work
pUG34-rrp44(1-475)	HIS3, CEN/ARS, PMET25::yEGFP3-rrp44(1-475)	This work
pUG34-rrp44Δ(364-407)	HIS3, CEN/ARS, PMET25::yEGFP3-rrp44Δ(364-407)	This work
pUG34(1-363)(408-895)	HIS3, CEN/ARS, PMET25::yEGFP3-rrp44(1-363)(408-895)	This work
pUG34-rrp44(1-218)	HIS3, CEN/ARS, PMET25::yEGFP3-rrp44(1-218)	This work
pUG34-rrp44(263-475)	HIS3, CEN/ARS, PMET25::yEGFP3-rrp44(263-475)	This work
pUG34-rrp44(475-1001)	HIS3, ARS/CEN/ PMET25::yEGFP3-rrp44(475-1001)	This work
pUG34-rrp44(R397A,R398T)	HIS3, CEN/ARS, PMET25::yEGFP3-rrp44(R397A,R398T)	This work
pUG34-rrp44(P187A,Y188A)	HIS3, CEN/ARS, PMET25::yEGFP3-rrp44(P187A,Y188A)	This work
YCplac33-GAL-A-RRP44	URA3,ARS/CEN/ PGAL1::ProtA-RRP44	This work
pGEX4T1	GST, AmpR	GE Healthcare
pET28-KAP95	His::KAP95, KanR	12
pET29-SRP1	His::SRP1, KanR	12
pGEX-RRP44	GST::RRP44, AmpR	Bagatelli and Oliveira, unpublished data
pGEMT-easy	lacZ	Promega

Table 2
Yeast strains

Name	Genotype	Reference
RRP41-TAP	*MATa his3Δ1 leu2Δ0 met15Δ0 ura3Δ0*	60
RRP6-TAP	*MATa his3Δ1 leu2Δ0 met15Δ0 ura3Δ0*	60
RRP43-TAP	*MATa his3Δ1 leu2Δ0 met15Δ0 ura3Δ0*	60
RPA190-mCherry (OGT8-1a)	*MATa his3Δ1 leu2Δ0 met15Δ0 ura3Δ0 RPA190-mCherry-URA3(Kl)*	This work
BY4742	*MATa his3Δ1 leu2Δ0 lys2Δ0 ura3Δ0*	EUROSCARF
BY4742-Nup57 tDimer (yEO4-1a)	*MATa his3Δ1 leu2Δ0 lys2Δ0 ura3Δ0 NUP57-tDimer-LEU2*	This work
Rrp6-GFP (yEO9-1a)	*MATa his3Δ1 leu2Δ0 met15Δ0 ura3Δ0 Rrp6 GFP-URA3*	This work
Rrp6-mCherry (yOE10-1a)	*MATa his3Δ1 leu2Δ0 met15Δ0 ura3Δ0 Rrp6 mCherry-URA3*	This work
Rrp41-GFP (yOE11-1a)	*MATa his3Δ1 leu2Δ0 met15Δ0 ura3Δ0 Rrp41 GFP-URA3*	This work
Rrp41-mCherry (yOE12-1a)	*MATa his3Δ1 leu2Δ0 met15Δ0 ura3Δ0 Rrp41 mCherry-URA3*	This work
Rrp43-GFP (yOE13-1a)	*MATa his3Δ1 leu2Δ0 met15Δ0 ura3Δ0 Rrp43 GFP-URA3*	This work
Rrp43-mCherry (yOE14-1a)	*MATa his3Δ1 leu2Δ0 met15Δ0 ura3Δ0 Rrp43 mCherry-URA3*	This work
Rrp44-GFP (yOE15-1a)	*MATa his3Δ1 leu2Δ0 met15Δ0 ura3Δ0 Rrp44 GFP-URA3*	This work
Rrp44-mCherry (yOE16-1a)	*MATa his3Δ1 leu2Δ0 met15Δ0 ura3Δ0 Rrp44 mCherry-URA3*	This work
Rrp6-GFP-RPA190mCherry (yOE17-1a)	*MATa his3Δ1 leu2Δ0 met15Δ0 ura3Δ0 Rrp6 GFP-URA3 RPA190mCherry-HIS3*	This work
Rrp41-GFP RPA190mCherry (yOE18-1a)	*MATa his3Δ1 leu2Δ0 met15Δ0 ura3Δ0 Rrp41 GFP-URA3 RPA190mCherry-HIS4*	This work
Rrp43-GFP RPA190mCherry (yOE19-1a)	*MATa his3Δ1 leu2Δ0 met15Δ0 ura3Δ0 Rrp43 GFP-URA3 RPA190mCherry-HIS5*	This work
Rrp44-GFP RPA190mCherry (yOE20-1a)	*MATa his3Δ1 leu2Δ0 met15Δ0 ura3Δ0 Rrp44 GFP-URA3 RPA190mCherry-HIS6*	This work
BY4741	*MATa his3Δ1 leu2Δ0 met15Δ0 ura3Δ0*	Euroscarf
Δsrp1 (FGY-41)	*YNL189w::kanMX4; his3Δ1; leu2Δ0; lys2Δ0; ura3Δ0; Ycplac33-GAL-A-SRP1*	12
ΔΔap95 (FGY-53)	*YLR347c::kanMX4; his3Δ1; leu2Δ0; lys2Δ0; ura3Δ0; Ycplac33-GAL-A-KAP95*	12
Δrrp6 (FGY-88)	*BY4742; Mat a; his3Δ1; leu2Δ0; lys2Δ0; ura3Δ0; YOR001w::kanMX4*	EUROSCARF
Δrrp44 (2n) (FGY-62)	*BY4743; MATa/MATα; ura3Δ0/ura3Δ0; leu2Δ0/leu2Δ0; his3Δ1/his3Δ1; met15Δ0/MET15; LYS2/lys2Δ0; YOL021c/YOL021c::kanMX4*	EUROSCARF
Δrrp44/YCplac33-GAL::A-RRP44 (FGY-90)	*ura3Δ0; leu2Δ0; his3Δ1/; met15Δ0/MET15; LYS2/lys2Δ0; YOL021c::kanMX5 YCplac33-GAL-A-RRP44*	This work
BY4742 (FGY-76)	*Matα; his3Δ1; leu2Δ0; lys2Δ0; ura3Δ0*	EUROSCARF
Δsxm1 (FGY-86)	*BY4742; Mata; his3Δ1; leu2Δ0; lys2Δ0; ura3Δ0; YDR395w::kanMX4*	EUROSCARF
Δkap114 (FGY-60)	*BY4742; Mata; his3Δ1; leu2Δ0; lys2Δ0; ura3Δ0; YGL241w::kanMX4*	EUROSCARF
Δkap123 (FGY-61)	*BY4742; Mata; his3Δ1; leu2Δ0; lys2Δ0; ura3Δ0; YER110C::kanMX4*	EUROSCARF

genomic loci, and analyzed by fluorescence microscopy. BY4742 strains bearing Rrp44 fused to GFP or mCherry were constructed as described (62). Similarly, Rpa190 fused to mCherry was constructed as described (62).

RPA190 was also genomic tagged with mCherry in exosome GFP-tagged strains and BY4742 strain. The same strategy was used by first amplifying the plasmid pFA6-mCherry-HIS3, then inserting it in the genome by homologous recombination and selecting for histidine prototrophy.

Nuclear localization signal identification

The software packages PSORT II Prediction (RRID:SCR_018772), cNLS Mapper (70), and NLStradamus (63) were used

to predict the presence of NLSs in the amino acidic sequence of Rrp44.

Fluorescence microscopy on fixed cells

For protein depletion based on *GAL1* promoter, cells were inoculated either in selective galactose or glucose medium and incubated for 14 to 16 h to exponential phase. For microscopy analysis, cells were fixed in 70% methanol for 15 min, rinsed with cold PBS, and then treated with 1 mg/ml of RNase for 30 min. Cells were observed using a Nikon Eclipse Ti microscope equipped with filters for green fluorescence (GFP-3035B-000-ZERO, Semrock) and red fluorescence (Texas Red BrightLine set, TXRED4040-B, Semrock). The exposure times varied from 1 to 3 s. Images were processed and analyzed using the programs Nis Elements (version 3.07; Nikon) and ImageJ (National Institutes of Health, Bethesda, MD). Confocal images were captured in a 1024 × 1024-pixel format using a Zeiss LSM 780 confocal laser-scanning inverted microscope (Carl Zeiss, Germany) at the Research Facility Center (CEFAP-USP). Image stacks comprised eight images captured with a αPlan-Apochromat ×100/1.46 oil differential interference contrast M27 objective (Carl Zeiss), applying a zoom factor of 1.5. Step intervals along the *z* axis ranged from 200 to 250 nm. Image processing was performed using Zen 2011 software (version 11.00.190; Carl Zeiss).

Fluorescence microscopy on living cells

Exponentially growing yeast were collected, resuspended in synthetic complete medium (DIFCO), and observed in the fluorescence microscope. Confocal microscopy was performed using a Nipkow-disk confocal system (Revolution; Andor) installed on an Olympus microscope (IX-81), featuring a confocal spinning disk unit (CSU22; Yokogawa) and a cooled electron multiplying charge-coupled device camera (DU 888; Andor). The system was controlled using IQ 2 software (Andor). Images were acquired using a ×100 Plan Apo 1.4 NA oil immersion objective and a 2-fold lens in the optical path. Single laser lines used for excitation were diode-pumped solid-state lasers exciting GFP fluorescence at 488 nm (50 milliwatt; Coherent) and mCherry fluorescence at 561 nm (50 milliwatt; Cobolt jive), and a Dichroic mirror Di01-T405/488/568/647-13x15x0,5 was used; Semrock was used and a bi-bandpass emission filter (FF01-512/630-25; Semrock) allowed collection of the green and red fluorescence. In our conditions, pixel size was 65 nm. For quantification of nucleolar volume, *z* stacks of 40 images with a 200-nm *z* step were used. Exposure times varied from 0.1 to 1 s. Digital pictures were processed using ImageJ (National Institutes of Health, Bethesda, MD) (RRID:SCR_003070).

Image analysis and quantification

Confocal images were imported into ImageJ, signal intensities of GFP-tagged proteins were measured and their subnuclear localizations were analyzed using a dedicated image analysis pipeline (ImageJ Macro). Cell area was determined based on transmission light thanks to the following steps: background removal (subtracting Gaussian Blur image – σ = 40); segmentation of the cells with Moments threshold algorithm; determination of the objects corresponding to the cells with Analyze Particle (ImageJ function); and separation of the cells in contact with Adjustable Watershed Plugin. Nucleolar and nuclear segmentation was achieved using the largest RNA polymerase I subunit Rpa190 tagged with mCherry, strongly enriched in the nucleolus, and detectable in the nucleoplasm. First, we applied a Sum Z-Projection to the initial mCherry Image. Then, to determine the nucleolus area in each cell, we used a Wavelet filter and finally segmented with a Yen threshold algorithm. To determine the nucleus area, we directly segmented on the *Z*-projected image a Triangle threshold algorithm. Cells were then divided in the nucleolus, nucleoplasm, and cytoplasm. ImageJ macro was used to quantify the GFP signal in each compartment. All quantifications were performed relative to background fluorescence, measured using control cells with Rpa190 tagged with mCherry, but with no GFP expression.

To quantify exosome signal enrichment in each compartment, the mean signal of the entire cell was calculated: ((intensity of gray level in the cell – background)/cell surface area). The mean cellular signal was used as a proxy to a homogeneous concentration in the entire cell. Each compartment mean signal measure was then divided by the mean cellular signal in each cell. The concentration ratio shows the enrichment of exosome signal per compartment, all relative to the mean signal of the entire cell.

Protein pulldown

Cellular extracts (generated in 20 mM Tris, 150 mM NaCl, 1 mM EDTA, 0.8% Nonidet, 1 mM DTT) of *Escherichia coli* cells expressing either GST or GST-Rrp44 were incubated for 2 h at 4 °C with 60 μl of GSH-Sepharose beads (GE Healthcare), the unbound material was collected and the beads washed with the same buffer. Beads were then incubated with cellular extracts containing His-Srp1 or His-Kap95, flow-through was collected, and beads were washed with the same buffer. Bound proteins were eluted with 50 mM Tris, pH 8.0, 10 mM reduced GSH.

Co-immunoprecipitation

Interaction of karyopherins Srp1 and kap95 with Rrp44 was tested by co-immunoprecipitation using strains Δ*kap95/GAL::A-KAP95* and Δ*srp1/GAL::A-SRP1* transformed with pUG34 or pUG34-Rrp44. For each strain, 2 liters of cells were grown to an OD600 ~1.0, and collected in co-IP buffer (0.1% Nonidet P-40, 150 mM NaCl, 5 mM EDTA, 50 mM Tris-HCl, pH 7.5, 0.5× Halt Protease Inhibitor mixture (Thermo Scientific) (modified from Ref. 64). Total yeast extracts were obtained with a Ball Mill device (Retsch, Mixer Mill MM 200 or Mixer Mill PM 100), and cleared by centrifugation at 40,000 rpm for 1 h at 4 °C. Supernatant was then incubated for 2 h at 4 °C with IgG-Sepharose 6 Fast Flow (GE Healthcare) previously equilibrated with co-IP buffer. The resin was washed four times with 500 μl of co-IP buffer (twice with 150 mM NaCl and twice with 250 mM NaCl), followed by a further wash with 100 mM ammonia acetate, 0.1 M magnesium chloride. Elution of the specific karyopherin was performed by incubation with 500 mM ammonium hydroxide for 20 min (65).

Immunoblotting experiments

Protein samples were resolved by SDS-PAGE and transferred to polyvinylidene difluoride or nitrocellulose membranes (GE Healthcare). Membranes were incubated with primary antibodies against GST (Sigma-Aldrich), His tag (Sigma-Aldrich), GFP (Sigma-Aldrich), or Pgk1 (Abcam) in PBS (PBS)/Tween 20/nonfat milk. Secondary antibodies used were anti-rabbit (IRDye 680RD) or anti-mouse IgG (IRDye 800CW) conjugated to fluorophore (Licor). Western blots were developed using Odyssey® Imaging Systems.

Northern hybridization

Total RNA was isolated from yeast cells by a modified hot phenol method (66). The RNA extract was quantified and 6 μg of denatured total RNA was loaded on gel. RNAs were separated by electrophoresis on 7% denaturing polyacrylamide gel, and transferred to Hybond nylon membrane (GE Healthcare). Hybridization was performed using biotin-labeled or fluorescent probes specific to rRNAs. 5S rRNA and scR1 were used as controls. Quantification of bands from Northern hybridizations was performed with ImageJ software.

Data availability

All data are contained within the manuscript.

Acknowledgments—We are grateful to all members of the Oliveira laboratory for help, reagents, and discussion, especially L. P. P. Cepeda. We thank Frederico Gueiros Filho and members of his laboratory for the use of the fluorescence microscope. We also thank Mario Costa Cruz from CEFAP-USP for help with confocal microscopy and discussion. We are very grateful to Sylvain Cantaloube from the LITC imaging platform of Toulouse TRI and Image processing platform for his assistance and development of the image analysis pipeline. We acknowledge members of the Gadal's lab for help, advice and discussion, especially Isabelle Leger-Silvestre, Christophe Dez, and Lise Dauban.

Author contributions—E. K. O., F. A. G.-Z., and C. C. O. conceptualization; E. K. O. and O. G. resources; E. K. O., F. A. G.-Z., O. G., and C. C. O. formal analysis; E. K. O. and F. A. G.-Z. validation; E. K. O. investigation; E. K. O., F. A. G.-Z., O. G., and C. C. O. writing-original draft; O. G. software; O. G. and C. C. O. funding acquisition; C. C. O. supervision.

Funding and additional information—This work was supported by Fundação de Amparo à Pesquisa do Estado de São Paulo (FAPESP) Grant- 15/06477-9 (to C. C. O.), and the Centre de Biologie Integrative, Toulouse (to O. G.). E. K. O. was supported by CNPq and FAPESP Fellowship Master's 17/17777-9, Research Internships Abroad Grant 18/19451-6, and the Centre National de la Recherche Scientifique). F. A. G.-Z. was suppported by FAPESP postdoctoral fellowship 12/50196-6.

Conflict of interest—The authors declare that they have no conflicts of interest with the contents of this article.

Abbreviations—The abbreviations used are: snoRNA, small nucleolar RNA; NLS, nuclear localization signal; DIC, differential interference contrast; IP, immunoprecipitation; DAPI, 4′,6-diamidino-2-phenylindole.

References

1. Chlebowski, A., Lubas, M., Jensen, T. H., and Dziembowski, A. (2013) RNA decay machines: the exosome. *Biochim. Biophys. Acta* **1829,** 552–560 CrossRef Medline
2. Schneider, C., and Tollervey, D. (2013) Threading the barrel of the RNA exosome. *Trends Biochem. Sci.* **38,** 485–493 CrossRef Medline
3. Januszyk, K., and Lima, C. D. (2014) The eukaryotic RNA exosome. *Curr. Opin. Struct. Biol.* **24,** 132–140 CrossRef Medline
4. Liu, Q., Greimann, J. C., and Lima, C. D. (2006) Reconstitution, activities, and structure of the eukaryotic RNA exosome. *Cell* **127,** 1223–1237 CrossRef Medline
5. Dziembowski, A., Lorentzen, E., Conti, E., and Séraphin, B. (2007) A single subunit, Dis3, is essentially responsible for yeast exosome core activity. *Nat. Struct. Mol. Biol.* **14,** 15–22 CrossRef Medline
6. Lebreton, A., Tomecki, R., Dziembowski, A., and Séraphin, B. (2008) Endonucleolytic RNA cleavage by a eukaryotic exosome. *Nature* **456,** 993–996 CrossRef Medline
7. Briggs, M. W., Burkard, K. T., and Butler, J. S. (1998) Rrp6p, the yeast homologue of the human PM-Scl 100-kDa autoantigen, is essential for efficient 5.8 S rRNA 3' end formation. *J. Biol. Chem.* **273,** 13255–13263 CrossRef Medline
8. Allmang, C., Kufel, J., Chanfreau, G., Mitchell, P., Petfalski, E., and Tollervey, D. (1999) Functions of the exosome in rRNA, snoRNA and snRNA synthesis. *EMBO J.* **18,** 5399–5410 CrossRef Medline
9. Allmang, C., Petfalski, E., Podtelejnikov, A., Mann, M., Tollervey, D., and Mitchell, P. (1999) The yeast exosome and human PM-Scl are related complexes of 3' → 5' exonucleases. *Genes Dev.* **13,** 2148–2158 CrossRef Medline
10. Burkard, K. T., and Butler, J. S. (2000) A nuclear 3'-5' exonuclease involved in mRNA degradation interacts with poly(A) polymerase and the hnRNA protein Npl3p. *Mol. Cell Biol.* **20,** 604–616 CrossRef Medline
11. Jin, R., Dobry, C. J., McCown, P. J., and Kumar, A. (2008) Large-scale analysis of yeast filamentous growth by systematic gene disruption and overexpression. *Mol. Biol. Cell* **19,** 284–296 CrossRef Medline
12. Gonzales-Zubiate, F. A., Okuda, E. K., Da Cunha, J. P. C., and Oliveira, C. C. (2017) Identification of karyopherins involved in the nuclear import of RNA exosome subunit Rrp6 in *Saccharomyces cerevisiae*. *J. Biol. Chem.* **292,** 12267–12284 CrossRef Medline
13. Fatica, A., and Tollervey, D. (2002) Making ribosomes. *Curr. Opin. Cell Biol.* **14,** 313–318 CrossRef Medline
14. Kressler, D., Linder, P., and de La Cruz, J. (1999) Protein trans-acting factors involved in ribosome biogenesis in *Saccharomyces cerevisiae*. *Mol. Cell Biol.* **19,** 7897–7912 CrossRef Medline
15. Mitchell, P., Petfalski, E., Shevchenko, A., Mann, M., and Tollervey, D. (1997) The exosome: a conserved eukaryotic RNA processing complex containing multiple 3'→5' exoribonucleases. *Cell* **91,** 457–466 CrossRef Medline
16. Zhang, L., Wu, C., Cai, G., Chen, S., and Ye, K. (2016) Stepwise and dynamic assembly of the earliest precursors of small ribosomal subunits in yeast. *Genes Dev.* **30,** 718–732 CrossRef Medline
17. Gasse, L., Flemming, D., and Hurt, E. (2015) Coordinated ribosomal ITS2 RNA processing by the Las1 complex integrating endonuclease, polynucleotide kinase, and exonuclease activities. *Mol. Cell* **60,** 808–815 CrossRef Medline
18. Konikkat, S., and Woolford, J. L., Jr. (2017) Principles of 60S ribosomal subunit assembly emerging from recent studies in yeast. *Biochem. J.* **474,** 195–214 CrossRef Medline
19. Fromm, L., Falk, S., Flemming, D., Schuller, J. M., Thoms, M., Conti, E., and Hurt, E. (2017) Reconstitution of the complete pathway of ITS2 processing at the pre-ribosome. *Nat. Commun.* **8,** 1787 CrossRef Medline
20. Dez, C., Houseley, J., and Tollervey, D. (2006) Surveillance of nuclear-restricted pre-ribosomes within a subnucleolar region of *Saccharomyces cerevisiae*. *EMBO J.* **25,** 1534–1546 CrossRef Medline

21. Choque, E., Schneider, C., Gadal, O., and Dez, C. (2018) Turnover of aberrant pre-40S pre-ribosomal particles is initiated by a novel endonucleolytic decay pathway. *Nucleic Acids Res.* **46,** 4699–4714 CrossRef Medline
22. Darrière, T., Pilsl, M., Sarthou, M. K., Chauvier, A., Genty, T., Audibert, S., Dez, C., Léger-Silvestre, I., Normand, C., Henras, A. K., Kwapisz, M., Calvo, O., Fernández-Tornero, C., Tschochner, H., and Gadal, O. (2019) Genetic analyses led to the discovery of a super-active mutant of the RNA polymerase I. *PLoS Genet.* **15,** e1008157 CrossRef Medline
23. Rodríguez-Galán, O., García-Gómez, J. J., Kressler, D., and de la Cruz, J. (2015) Immature large ribosomal subunits containing the 7S pre-rRNA can engage in translation in *Saccharomyces cerevisiae*. *RNA Biol.* **12,** 838–846 CrossRef Medline
24. Huh, W. K., Falvo, J. V., Gerke, L. C., Carroll, A. S., Howson, R. W., Weissman, J. S., and O'Shea, E. K. (2003) Global analysis of protein localization in budding yeast. *Nature* **425,** 686–691 CrossRef Medline
25. Zanchin, N. I., and Goldfarb, D. S. (1999) Nip7p interacts with Nop8p, an essential nucleolar protein required for 60S ribosome biogenesis, and the exosome subunit Rrp43p. *Mol. Cell Biol.* **19,** 1518–1525 CrossRef Medline
26. Süel, K. E., Gu, H., and Chook, Y. M. (2008) Modular organization and combinatorial energetics of proline-tyrosine nuclear localization signals. *PLos Biol.* **6,** e137 CrossRef Medline
27. Lee, C., Hodgins, D. C., Calvert, J. G., Welch, S. K., Jolie, R., and Yoo, D. (2006) The nuclear localization signal of the PRRS virus nucleocapsid protein viral replication *in vitro* and antibody response *in vivo*. *Adv. Exp. Med. Biol.* **581,** 145–148 CrossRef Medline
28. Süel, K. E., and Chook, Y. M. (2009) Kap104p imports the PY-NLS-containing transcription factor Tfg2p into the nucleus. *J. Biol. Chem.* **284,** 15416–15424 CrossRef Medline
29. Fries, T., Betz, C., Sohn, K., Caesar, S., Schlenstedt, G., and Bailer, S. M. (2007) A novel conserved nuclear localization signal is recognized by a group of yeast importins. *J. Biol. Chem.* **282,** 19292–19301 CrossRef Medline
30. Graham, A. C., Davis, S. M., and Andrulis, E. D. (2009) Interdependent nucleocytoplasmic trafficking and interactions of Dis3 with Rrp6, the core exosome and importin-α3. *Traffic* **10,** 499–513 CrossRef Medline
31. Mamolen, M., Smith, A., and Andrulis, E. D. (2010) *Drosophila melanogaster* Dis3 N-terminal domains are required for ribonuclease activities, nuclear localization and exosome interactions. *Nucleic Acids Res.* **38,** 5507–5517 CrossRef Medline
32. Houseley, J., LaCava, J., and Tollervey, D. (2006) RNA-quality control by the exosome. *Nat. Rev. Mol. Cell Biol.* **7,** 529–539 CrossRef Medline
33. Ho, Y., Gruhler, A., Heilbut, A., Bader, G. D., Moore, L., Adams, S. L., Millar, A., Taylor, P., Bennett, K., Boutilier, K., Yang, L., Wolting, C., Donaldson, I., Schandorff, S., Shewnarane, J., *et al.* (2002) Systematic identification of protein complexes in *Saccharomyces cerevisiae* by mass spectrometry. *Nature* **415,** 180–183 CrossRef Medline
34. Krogan, N. J., Cagney, G., Yu, H., Zhong, G., Guo, X., Ignatchenko, A., Li, J., Pu, S., Datta, N., Tikuisis, A. P., Punna, T., Peregrin-Alvarez, J. M., Shales, M., Zhang, X., Davey, M., *et al.* (2006) Global landscape of protein complexes in the yeast *Saccharomyces cerevisiae*. *Nature* **440,** 637–643 CrossRef Medline
35. Aloy, P., Ciccarelli, F. D., Leutwein, C., Gavin, A. C., Superti-Furga, G., Bork, P., Bottcher, B., and Russell, R. B. (2002) A complex prediction: three-dimensional model of the yeast exosome. *EMBO Rep.* **3,** 628–635 CrossRef Medline
36. Kilchert, C., Wittmann, S., and Vasiljeva, L. (2016) The regulation and functions of the nuclear RNA exosome complex. *Nat. Rev. Mol. Cell Biol.* **17,** 227–239 CrossRef Medline
37. Tran, E. J., King, M. C., and Corbett, A. H. (2014) Macromolecular transport between the nucleus and the cytoplasm: advances in mechanism and emerging links to disease. *Biochim. Biophys. Acta* **1843,** 2784–2795 CrossRef Medline
38. Drazkowska, K., Tomecki, R., Stodus, K., Kowalska, K., Czarnocki-Cieciura, M., and Dziembowski, A. (2013) The RNA exosome complex central channel controls both exonuclease and endonuclease Dis3 activities *in vivo* and *in vitro*. *Nucleic Acids Res.* **41,** 3845–3858 CrossRef Medline
39. Makino, D. L., Schuch, B., Stegmann, E., Baumgärtner, M., Basquin, C., and Conti, E. (2015) RNA degradation paths in a 12-subunit nuclear exosome complex. *Nature* **524,** 54–58 CrossRef Medline
40. Wang, H. W., Wang, J., Ding, F., Callahan, K., Bratkowski, M. A., Butler, J. S., Nogales, E., and Ke, A. (2007) Architecture of the yeast Rrp44 exosome complex suggests routes of RNA recruitment for 3' end processing. *Proc. Natl. Acad. Sci. U.S.A.* **104,** 16844–16849 CrossRef Medline
41. Zinder, J. C., Wasmuth, E. V., and Lima, C. D. (2016) Nuclear RNA exosome at 3.1 A reveals substrate specificities, RNA paths, and allosteric inhibition of Rrp44/Dis3. *Mol. Cell* **64,** 734–745 CrossRef Medline
42. Das, B., Butler, J. S., and Sherman, F. (2003) Degradation of normal mRNA in the nucleus of *Saccharomyces cerevisiae*. *Mol. Cell Biol.* **23,** 5502–5515 CrossRef Medline
43. Oliveira, C. C., Gonzales, F. A., and Zanchin, N. I. (2002) Temperature-sensitive mutants of the exosome subunit Rrp43p show a deficiency in mRNA degradation and no longer interact with the exosome. *Nucleic Acids Res.* **30,** 4186–4198 CrossRef Medline
44. Zhang, E., Khanna, V., Dacheux, E., Namane, A., Doyen, A., Gomard, M., Turcotte, B., Jacquier, A., and Fromont-Racine, M. (2019) A specialised SKI complex assists the cytoplasmic RNA exosome in the absence of direct association with ribosomes. *EMBO J.* **38,** e100640 CrossRef Medline
45. Collart, M. A. (2003) Global control of gene expression in yeast by the Ccr4-Not complex. *Gene* **313,** 1–16 CrossRef Medline
46. Azzouz, N., Panasenko, O. O., Colau, G., and Collart, M. A. (2009) The CCR4-NOT complex physically and functionally interacts with TRAMP and the nuclear exosome. *PLoS ONE* **4,** e6760 CrossRef Medline
47. Beelman, C. A., Stevens, A., Caponigro, G., LaGrandeur, T. E., Hatfield, L., Fortner, D. M., and Parker, R. (1996) An essential component of the decapping enzyme required for normal rates of mRNA turnover. *Nature* **382,** 642–646 CrossRef Medline
48. Boeck, R., Lapeyre, B., Brown, C. E., and Sachs, A. B. (1998) Capped mRNA degradation intermediates accumulate in the yeast spb8-2 mutant. *Mol. Cell Biol.* **18,** 5062–5072 CrossRef Medline
49. Hsu, C. L., and Stevens, A. (1993) Yeast cells lacking 5'→3' exoribonuclease 1 contain mRNA species that are poly(A) deficient and partially lack the 5' cap structure. *Mol. Cell Biol.* **13,** 4826–4835 CrossRef Medline
50. Raijmakers, R., Schilders, G., and Pruijn, G. J. (2004) The exosome, a molecular machine for controlled RNA degradation in both nucleus and cytoplasm. *Eur. J. Cell Biol.* **83,** 175–183 CrossRef Medline
51. Klinge, S., and Woolford, J. L., Jr. (2019) Ribosome assembly coming into focus. *Nat. Rev. Mol. Cell Biol.* **20,** 116–131 CrossRef Medline
52. Kornprobst, M., Turk, M., Kellner, N., Cheng, J., Flemming, D., Koš-Braun, I., Kos, M., Thoms, M., Berninghausen, O., Beckmann, R., and Hurt, E. (2016) Architecture of the 90S Pre-ribosome: a structural view on the birth of the eukaryotic ribosome. *Cell* **166,** 380–393 CrossRef Medline
53. Barandun, J., Hunziker, M., and Klinge, S. (2018) Assembly and structure of the SSU processome: a nucleolar precursor of the small ribosomal subunit. *Curr. Opin. Struct. Biol.* **49,** 85–93 CrossRef Medline
54. Thoms, M., Thomson, E., Baëler, J., Gnädig, M., Griesel, S., and Hurt, E. (2015) The exosome is recruited to RNA substrates through specific adaptor proteins. *Cell* **162,** 1029–1038 CrossRef Medline
55. Cepeda, L. P. P., Bagatelli, F. F. M., Santos, R. M., Santos, M. D. M., Nogueira, F. C. S., and Oliveira, C. C. (2019) The ribosome assembly factor Nop53 controls association of the RNA exosome with pre-60S particles in yeast. *J. Biol. Chem.* **294,** 19365–19380 CrossRef Medline
56. Yao, R. W., Xu, G., Wang, Y., Shan, L., Luan, P. F., Wang, Y., Wu, M., Yang, L. Z., Xing, Y. H., Yang, L., and Chen, L. L. (2019) Nascent pre-rRNA sorting via phase separation drives the assembly of dense fibrillar components in the human nucleolus. *Mol. Cell* **76,** 767–783.e11 CrossRef Medline
57. Niedenthal, R. K., Riles, L., Johnston, M., and Hegemann, J. H. (1996) Green fluorescent protein as a marker for gene expression and subcellular localization in budding yeast. *Yeast* **12,** 773–786 CrossRef
58. Wang, R., Kamgoue, A., Normand, C., Leger-Silvestre, I., Mangeat, T., and Gadal, O. (2016) High resolution microscopy reveals the nuclear shape of budding yeast during cell cycle and in various biological states. *J. Cell Sci.* **129,** 4480–4495 CrossRef Medline

59. Laporte, D., Courtout, F., Tollis, S., and Sagot, I. (2016) Quiescent *Saccharomyces cerevisiae* forms telomere hyperclusters at the nuclear membrane vicinity through a multifaceted mechanism involving Esc1, the Sir complex, and chromatin condensation. *Mol. Biol. Cell* **27,** 1875–1884 CrossRef Medline
60. Ghaemmaghami, S., Huh, W. K., Bower, K., Howson, R. W., Belle, A., Dephoure, N., O'Shea, E. K., and Weissman, J. S. (2003) Global analysis of protein expression in yeast. *Nature* **425,** 737–741 CrossRef Medline
61. Sung, M. K., Ha, C. W., and Huh, W. K. (2008) A vector system for efficient and economical switching of C-terminal epitope tags in *Saccharomyces cerevisiae*. *Yeast* **25,** 301–311 CrossRef Medline
62. Longtine, M. S., McKenzie, A., 3rd, Demarini, D. J., Shah, N. G., Wach, A., Brachat, A., Philippsen, P., and Pringle, J. R. (1998) Additional modules for versatile and economical PCR-based gene deletion and modification in *Saccharomyces cerevisiae*. *Yeast* **14,** 953–961 CrossRef
63. Nguyen Ba, A. N., Pogoutse, A., Provart, N., and Moses, A. M. (2009) NLStradamus: a simple Hidden Markov Model for nuclear localization signal prediction. *BMC Bioinformatics* **10,** 202 CrossRef Medline
64. Bakhrat, A., Baranes, K., Krichevsky, O., Rom, I., Schlenstedt, G., Pietrokovski, S., and Raveh, D. (2006) Nuclear import of ho endonuclease utilizes two nuclear localization signals and four importins of the ribosomal import system. *J. Biol. Chem*. **281,** 12218–12226 CrossRef Medline
65. Ohmayer, U., Gamalinda, M., Sauert, M., Ossowski, J., Pöll, G., Linnemann, J., Hierlmeier, T., Perez-Fernandez, J., Kumcuoglu, B., Leger-Silvestre, I., Faubladier, M., Griesenbeck, J., Woolford, J., Tschochner, H., and Milkereit, P. (2013) Studies on the assembly characteristics of large subunit ribosomal proteins in *S. cerevisae*. *PLoS ONE* **8,** e68412 CrossRef Medline
66. Gonzales, F. A., Zanchin, N. I., Luz, J. S., and Oliveira, C. C. (2005) Characterization of *Saccharomyces cerevisiae* Nop17p, a novel Nop58p-interacting protein that is involved in Pre-rRNA processing. *J. Mol. Biol.* **346,** 437–455 CrossRef Medline
67. Bachellier-Bassi, S., Gadal, O., Bourout, G., and Nehrbass, U. (2008) Cell cycle-dependent kinetochore localization of condensin complex in *Saccharomyces cerevisiae*. *J. Struct. Biol*. **162,** 248–259 CrossRef Medline
68. Hellmuth, K., Lau, D. M., Bischoff, F. R., Kunzler, M., Hurt, E., and Simos, G. (1998) Yeast Los1p has properties of an exportin-like nucleocytoplasmic transport factor for tRNA. *Mol. Cell Biol*. **18,** 6374–6386 CrossRef Medline
69. Berger, A. B., Cabal, G. G., Fabre, E., Duong, T., Buc, H., Nehrbass, U., Olivo-Marin, J. C., Gadal, O., and Zimmer, C. (2008) High-resolution statistical mapping reveals gene territories in live yeast. *Nat. Methods* **5,** 1031–1037 CrossRef Medline
70. Kosugi, S., Hasebe, M., Tomita, M., and Yanagaqwa, H. (2009) Systematic identification of cell cycle-dependent yeast nucleocytoplasmic shuttling proteins by prediction of composite motifs. *Proc. Natl. Acad. Sci. U.S.A.* **106,** 10171–10176 CrossRef Medline